Schimmelpfennig, I., Williams, A., Pik, R., Burnard, P., Niedermann, S., Finkel, R., Schneider, B., Benedetti, L. (2011): Inter-comparison of cosmogenic in-situ 3He, 21Ne and 36Cl at low latitude along an altitude transect on the SE slope of Kilimanjaro volcano (3°S, Tanzania). - Quaternary Geochronology, 6, 5, 425-436,

DOI: 10.1016/j.quageo.2011.05.002

Inter-comparison of cosmogenic in-situ ^{3}He, ^{21}Ne and ^{36}Cl at low latitude along an altitude transect on the SE slope of Kilimanjaro volcano (3°S, Tanzania)

Irene Schimmelpfennig[a,b*], Alice Williams[a], Raphaël Pik[a], Pete Burnard[a], Samuel Niedermann[c], Robert Finkel[b,d], Björn Schneider[e], Lucilla Benedetti[b]

[a] CRPG, UPR 2300 CNRS, Nancy Universités, 15 rue Notre Dame des Pauvres, 54501 Vandoeuvre-lès-Nancy, France

[b] CEREGE, UMR 6635 CNRS, Université Paul Cézanne, Europôle de l'Arbois, 13545 Aix en Provence, France

[c] Helmholtz-Zentrum Potsdam – Deutsches GeoForschungsZentrum GFZ, Telegrafenberg, 14473 Potsdam, Germany

[d] Earth and Planetary Science Department, University of California Berkeley, Berkeley, CA 94720-4767, USA

[e] Vrije Universiteit, Department of Isotope Geochemistry, de Boelelaan 1085, 1081 HV Amsterdam, The Netherlands

* corresponding author. Present address: LDEO, Columbia University, Route 9W, Palisades, NY 10964, USA; Tel.: ++1 845 365 8653; Fax: ++1 845 365 8155; E-mail: schimmel@ldeo.columbia.edu

Abstract

Because the intensity and energy spectrum of the cosmic ray flux are affected by atmospheric depth and geomagnetic-field strength, cosmogenic nuclide production rates increase considerably with altitude and to a lesser degree with latitude. The scaling methods used to account for spatial variability in production rates assume that all cosmogenic nuclides have the same altitude dependence. In this study we evaluate whether the production rates of cosmogenic ^{36}Cl, ^{3}He and ^{21}Ne change differently with altitude, which is plausible due to the different threshold energies of their production reactions. If so, nuclide-specific scaling factors would be required.

Concentrations of the three cosmogenic nuclides were determined in mafic phenocrysts over an altitude transect between 1000 and 4300 m at Kilimanjaro volcano (3° S). Altitude-dependence of relative production rates was assessed in two ways: by determination of concentration ratios and by calculation of apparent exposure age ratios for all nuclide pairs. The latter accounts for characteristics of ^{36}Cl that the stable nuclides ^{3}He and ^{21}Ne do not possess (radioactive decay, high sensitivity to mineral composition and significant contributions from production reactions other than spallation). All ratios overlap within error over the entire transect, and altitudinal variation in relative production rates is not therefore evident. This suggests that nuclide-specific scaling factors are not required for the studied nuclides at this low latitude location. However, because previous studies have documented anomalous altitude-dependent variations in ^{3}He production at mid-latitude sites, the effect of latitude on cross-calibrations should be further evaluated.

We determined cosmogenic ^{21}Ne/^{3}He concentration ratios of 0.1864 ± 0.0085 in pyroxenes and 0.377 ± 0.018 in olivines, agreeing with those reported in previous studies.

Despite the absence of independently determined ages for the studied lava surfaces, the consistency in the data-set should enable progress to be made in the determination of the production rates of all three nuclides as soon as the production rate of one of the nuclides has been accurately defined.

To our knowledge this is the first time that ^{36}Cl has been measured in pyroxene. The Cl extraction method was validated by measuring ^{36}Cl in co-existing plagioclase phenocrysts in one of the samples.

Key words: Cosmogenic nuclides; Chlorine-36, Helium-3, Neon-21; Cross-calibration; Pyroxene; Olivine; Kilimanjaro; Altitude dependent scaling

1. Introduction

Accurate application of the surface-exposure dating technique, using terrestrial cosmogenic nuclides (TCN) such as ^{36}Cl, ^{3}He, ^{21}Ne, ^{10}Be or ^{26}Al, requires precise and accurate knowledge of the production rate of the nuclide of interest (the number of atoms produced per gram of target material per year) and the variation of this production rate in space and time (scaling). Reference production rates have been determined to allow application of the TCN method anywhere on Earth (see review in Gosse and Phillips, 2001). These are extrapolated to a particular location using scaling factors calculated according to one of the published scaling models (e.g. Stone, 2000, Dunai, 2001a, Desilets and Zreda, 2003, Lifton et al., 2005). Experimental calibrations of reference production rates are made by (1) measuring the concentration of the nuclide of interest in a geological sample from an independently dated surface at a specific geographic location, and (2) scaling the calculated time-integrated local production rate to the traditional reference position at sea-level and high latitude (SLHL) and to the present (Gosse and Phillips, 2001).

It is clearly imperative that scaling methods accurately quantify the spatial and temporal variability of TCN production on Earth. Recently however, some authors have cast doubt on our understanding of this variability, suggesting it could be one of the main causes for inconsistencies between calibrated SLHL production rates, thereby constituting a major source of uncertainty in TCN exposure ages (Balco et al., 2008, 2009, Schimmelpfennig et al., 2011).

Published scaling methods generally assume that the scaling factor for a particular type of nuclear-reaction (neutron- or muon-induced) is valid for all TCN and independent of the target element on which the reaction occurs. For example, at any given location production of ^{10}Be by spallation of Si and O is scaled using the same factor as production of ^{36}Cl by

92 spallation of Ca. However, this approach is controversial and the need for nuclide specific
93 scaling factors, as first discussed by Dunai (2001b), is currently being debated. The argument
94 is based on two aspects of TCN production. First, excitation functions for the various TCN
95 production reactions are known to be different (e.g. Desilets et al., 2006, Amidon et al., 2008
96 and references therein). This means that the threshold energies (minimum energies of
97 secondary nucleons required for the reactions) and cross sections (probabilities of the
98 occurrence of the reaction at a certain nucleon energy) differ between the various production
99 reactions. Second, it has been hypothesized that the energy spectrum of the secondary
100 nucleons shifts towards lower energies with increasing atmospheric depth (Desilets and Zreda,
101 2003). For example, the threshold energy for the production of ^{36}Cl from spallation of K
102 (about 5 MeV) is lower than that from spallation of Ca (about 20 MeV; see excitation
103 functions in Fig. 2 in Desilets et al., 2006). It might therefore be expected that the ratio of ^{36}Cl
104 production from K to that from Ca will increase with increasing atmospheric depth (i.e.
105 decreasing altitude). If so, nuclide- and even target-element-specific scaling factors would be
106 needed.
107 One way of assessing TCN production and the global consistency in scaling is to determine
108 relative production rates of different TCN in geomorphic surfaces. These *cross-calibrations*
109 do not necessarily require that surfaces be independently dated nor perfectly preserved.
110 Measurements of multiple TCN in the same or in different mineral phases from a single
111 sample can be used to refine poorly known SLHL production rates using TCN with well-
112 constrained production rates (e.g. Amidon et al., 2009, Balco and Shuster, 2009, Goethals et
113 al., 2009). In addition, performing cross-calibrations over a range of altitudes, latitudes or
114 exposure times enables assessment of any spatial and/or temporal dependence in the
115 production of the different TCN. For example, Gayer et al. (2004) measured ^{3}He/^{10}Be in
116 Himalayan garnets over an altitude transect between 3000 and 4600 m and determined

117 production ratios higher than previously documented (Cerling and Craig, 1994). The apparent
118 ^{3}He overproduction, which seemed to be prevalent at high altitude, was tentatively attributed
119 to a significant difference in the threshold energies for the production of the two nuclides.
120 More recently, Dunai et al. (2007) considered a second cosmogenic ^{3}He production
121 mechanism, via low-energy neutron capture on ^{6}Li, to explain the higher ^{3}He production
122 reported in Gayer et al. (2004). Some later studies were unable to identify an altitude-
123 dependence unique to ^{3}He production (Blard et al., 2006, Vermeesch et al., 2009). In others,
124 higher than expected apparent ^{3}He production rates were also inferred: at high altitudes in the
125 Himalayas (Amidon et al., 2008) and on the Puna plateau in Argentina (Niedermann et al.,
126 2009), and even at lower altitudes in the Coso Volcanic field and the Bishop Tuff (both in
127 California, USA; Amidon et al., 2009, Niedermann et al., 2009).
128 In this study, we evaluate whether relative production rates of TCN change with altitude at a
129 low-latitude site (3°S) and if overproduction of ^{3}He at high altitudes occurs. We cross-
130 calibrate production of ^{3}He, ^{21}Ne and ^{36}Cl in lava-flow and glacial surfaces outcropping over
131 an altitude profile between 1000 and 4300 m, on the slopes of Mt. Kilimanjaro, Tanzania. All
132 three nuclides can be measured in clinopyroxene phenocrysts and this mineral phase provides
133 the most complete data set in this study. In addition, ^{3}He was measured in olivine phenocrysts
134 in all samples except one, and ^{21}Ne was measured in olivines at two different altitudes.
135 To our knowledge, this is the first time that ^{36}Cl has been measured in a mafic mineral phase.
136 To validate the method, ^{36}Cl was measured in plagioclase phenocrysts coexisting with
137 pyroxenes in one of the samples.
138
139

2. Geological setting and sampling

Based on an initial project objective of calibrating absolute and relative production rates of TCN at a low-latitude site and over a large altitude transect, sampling was undertaken in 2005 at Mount Kilimanjaro, Tanzania (3°S) (Fig. 1). This large shield volcano, Africa's highest mountain (5892 m), is located at the eastern end of the Ngorongoro-Kilimanjaro Volcanic Belt, which forms one arm of the triple rift-system that characterizes the eastern branch of the East African Rift System. Kilimanjaro consists of three NW-SE aligned volcanic peaks, Shira (3962 m), Kibo (5892 m) and Mawenzi (5149 m), constructed in multiple phases. The first phase took place between 2.5 Ma and 1.9 Ma at the Shira vent (Nonnotte et al., 2008). A large sector collapse signalled the end of this phase, after which volcanic activity shifted eastwards to the Kibo and Mawenzi peaks, at around 1 Ma. Activity at Mawenzi ceased around 500 ka, but continued at Kibo with two major periods of volcanic activity occurring between 460 ka and 340 ka. The final stages of volcanism at Kilimanjaro consisted of the eruption of basaltic flows and scoria from small parasitic cones located on the volcano flanks, between around 200 ka and 150 ka (Nonnotte et al., 2008).

For this study, we principally targeted cones and lava flows from this last volcanic period in a region known as the Rombo Zone, located on the south-eastern flank, south of Mawenzi Peak (Downie and Wilkinson, 1972). This zone comprises olivine- and pyroxene-rich basanitic and ankaramitic flows erupted from parasitic cones distributed over a large elevation range, from < 1500 to > 4500 m. Suitable exposure of lava-flow surfaces is limited however between 1700 and 2500 m due to the presence of a dense tropical rainforest (Fig. 1). Flow-top preservation is also compromised above ~ 3700 m as a result of significant glacial activity during the Quaternary (Shanahan and Zreda, 2000).

While an effort was made to sample pristine flow-top features for absolute calibration of TCN production rates, at many sites this was not possible. Between 2700 and 3200 m, well-preserved ropy tops of lava-flows (Fig. A1 in Appendix) out-crop at the bases of parasitic cones. However, accessing the inner, degassed parts of the flow in order to extract rock suitable for precise Ar/Ar or K/Ar dating was difficult, and most flows were also too small and thin to have well developed massive interiors. As such, our efforts to obtain independent ages and absolute production rates for these flows were unsuccessful. For the parasitic cones erupted in the Rombo Zone, the only precise published eruption ages are K/Ar ages of 165 ± 5 ka and 195 ± 5 ka for two basaltic flows (Nonnotte et al., 2008), but their surfaces were not appropriate for exposure dating. For the investigation of relative TCN production rates, however, it is possible to use surfaces, such as glacially-polished surfaces, for which the eruption age of the lava-flow is not necessarily equal to the apparent exposure age.

Eight surface samples were collected at six different altitudes between 1000 and 4300 m (Table 1 and Fig. 1). Half of the samples were taken from well-preserved surfaces of two lava-flows (TZ10, TZ12, TZ13 and TZ14), two from eroding surfaces (TZ09, TZ17) and two from glacially polished surfaces (TZ15, TZ19). Based on field observations, the maximum rock thickness removed from the lava-flow at the lowest sample site at 1013 m altitude (TZ09) is estimated to be 30 cm. The surface of sample TZ17 also appeared to be slightly degraded in the field and the outcrop was surrounded by scoria and gravel deposits. Sample TZ15 was taken from a glacially polished doleritic dyke bearing large plagioclase laths in addition to pyroxene and minor olivine. A formation age of 527 ± 3 ka was determined for the dyke by $^{39}Ar/^{40}Ar$ dating (see Appendix). The exposure age of the surface can be expected to be significantly younger. The highest sample (TZ19) also exhibits slight glacial polishing. More detailed descriptions and photographs of sample sites are given in the Appendix.

- Fig. 1 about here -

- Table 1 about here -

3. Methods

3. 1 Physical sample preparation

Prior to sample preparation, pieces of whole rock from each surface were set-aside for thin-section preparation and bulk-rock composition analyses. For TCN analyses, the top 5 to 10 cm of each whole rock sample was sawn off, then crushed and wet-sieved to remove dust particles and the finest grain sizes (< 125 μm). A hand-magnet was passed over all fractions to remove magnetic groundmass. Using a binocular microscope, olivine and pyroxene phenocrysts were hand-picked to obtain pure mineral separates, with care taken to ensure complete removal of altered crystals and crystals with adhering groundmass. For ^{36}Cl analyses, approximately 5 to 10 g of pure pyroxene phenocrysts were handpicked from the coarsest fractions. For sample TZ15, a Frantz magnetic separator was used to separate several grams of 0.5-mm sized plagioclase phenocrysts from the more magnetic mafic minerals. Plagioclases were handpicked in order to maximize sample purity. For noble gas extractions, approximately 2 g of the coarsest pure fractions were cleaned in acetone and set aside for in vacuo crushing and determination of magmatic helium isotope ratios. For the melt extractions, up to 3 g of phenocrysts from the 0.5 to 0.7 mm size fraction were cleaned in acetone, hand-crushed and sieved to 0.1 - 0.3 mm and then re-picked and cleaned once more in acetone, to ensure the highest degree of sample purity.

3. 2 Chemical ^{36}Cl extraction and measurement

Chemical extraction of ^{36}Cl was conducted at CEREGE (Aix en Provence, France). The procedure is detailed in the Appendix. Several procedural blanks were performed in order to assess cleanliness during chemical extraction and to correct sample measurements for laboratory ^{36}Cl and stable Cl sources.

Concentrations of ^{36}Cl and Cl were determined using the Lawrence Livermore National Laboratory FN accelerator mass spectrometer (LLNL-CAMS, USA). Isotope dilution (addition of a ^{35}Cl-enriched carrier) allows simultaneous determination of ^{36}Cl and Cl concentrations. ^{36}Cl/^{35}Cl ratios were determined by normalizing to a ^{36}Cl standard prepared by K. Nishiizumi (Sharma et al., 1990). The stable ratio ^{35}Cl/^{37}Cl was also normalized to this standard, assuming a natural ratio of 3.127. Measured ratios and their uncertainties are presented in Table A1 in the Appendix. The precision of the ^{35}Cl/^{37}Cl ratios accounts for 2% or less (standard deviation of repeat measurements). The precision of the ^{36}Cl/^{35}Cl ratios ranges from 2 to 7%.

Blank ^{36}Cl/^{35}Cl ratios range between 7×10^{-15} and 9×10^{-15}, and are one to two orders of magnitude lower than the sample ^{36}Cl/^{35}Cl ratios (Table A1). The resulting blank-corrected ^{36}Cl and Cl concentrations range from (0.63 to 5.25) $\times 10^{6}$ atoms ^{36}Cl g^{-1} and from 1 to 10 ppm Cl, respectively (Table A1). The ^{36}Cl concentrations are also given in Table 3.

3.3 Noble gas measurements

Helium measurements were carried out using the Helix Split Flight Tube and Helix Multi-collector mass spectrometers (GV instruments) at CRPG (Nancy, France) and a VG-5400 mass spectrometer at GFZ (Potsdam, Germany) (Table A3 in the Appendix shows where each measurement was made). Neon measurements were performed with the VG-5400 mass spectrometer at GFZ. While samples were degassed in a single step at CRPG, a two-step

heating procedure (900°C and 1750°C) was used at GFZ in order to separate a possible high atmospheric Ne component from the major cosmogenic fraction. Mass spectrometers were cross-calibrated by way of internal standard replication and measurement of CRONUS-EU mineral standards. Further details of these inter-comparisons and of the noble gas extraction and measurement procedures in the two laboratories can be found in the Appendix.

Determination of cosmogenic ^{3}He concentrations

Concentrations of cosmogenic ^{3}He in pyroxene and olivine are traditionally calculated from melt and crush measurements using an equation that corrects for the trapped (magmatic) He component (Kurz, 1986):

$$^3He_{cos} = {}^3He_m - {}^4He_m \times (^3He/^4He)_{mag} \qquad \text{Eq. 1}$$

where $^3He_{cos}$ is the cosmogenic ^{3}He concentration, ^3He_m and ^4He_m are the concentrations of ^{3}He and ^{4}He measured from melt extractions and $(^3He/^4He)_{mag}$ is the magmatic ^{3}He/^{4}He value, normally determined from phenocryst crush extractions. Because of insufficient sample material and low He yields, not all $(^3He/^4He)_{mag}$ values in this study were determined by crushing. Isochron intercepts according to the method by Blard and Pik (2008) were used for samples TZ17 and TZ19 (Fig. A2 in Appendix). For samples TZ09 and TZ15 the value for $(^3He/^4He)_{mag}$ was estimated. A description of the magmatic ^{3}He/^{4}He determinations is given in the Appendix.

A critical step in the determination of cosmogenic ^{3}He is the correction for the implanted or ingrown radiogenic ^{4}He (^{4}He*), which may be significant even in very young rocks (e.g. Dunai and Wijbrans, 2000, Blard and Farley, 2008, Blard and Pik, 2008). In this study, for partially eroded volcanic surfaces (TZ09 and TZ17) and glacially polished surfaces (TZ15 and

261 TZ19), $^{4}He^{*}$ was estimated from whole-rock and phenocryst U and Th concentrations
262 following Farley et al. (2006). The calculated $^{4}He^{*}$ was subtracted from the $^{4}He_{m}$ abundance
263 prior to using Eq. 1. For TZ09, TZ17 and TZ19, the magnitude of $^{4}He^{*}$ correction ranged
264 between 4% and 25% of total $^{4}He_{m}$; for pyroxene and olivine replicates of TZ15 it was
265 calculated to be 53% to 68% based on the rock formation age of ~525 ka (see discussion in
266 section 4.2). For the non-eroded volcanic surfaces (TZ10, 12, 13, 14) we applied the R-factor
267 correction of Blard and Pik (2008). The R-factor is a function of the production rate ratio
268 between $^{4}He^{*}$ and $^{3}He_{cos}$, which is constant over time for non-eroded volcanic surfaces, and
269 $(^{3}He/^{4}He)_{mag}$. The R-factor values for all four samples are > 0.98 (see Table A3 in the
270 Appendix), which corresponds to a $^{4}He^{*}$ correction of < 2%.
271 Helium data were systematically obtained for pyroxenes and olivines, except for sample TZ09
272 where only pyroxenes were available in sufficient quantity. Full raw data and calculated
273 cosmogenic ^{3}He concentrations are presented in Table A3. Concentrations of $^{3}He_{cos}$ range
274 from (9.6 to 99.8) × 10^{6} at g^{-1} in pyroxenes and from (13.1 to 97.9) × 10^{6} at g^{-1} in olivines.
275 Relative $^{3}He_{cos}$ production in the two minerals is compared in Fig. 2. As observed in previous
276 studies (e.g. Blard et al., 2005, Fenton et al., 2009), for most samples, cosmogenic ^{3}He
277 concentrations in cogenetic olivines and pyroxenes are identical within analytical uncertainty.
278 The exceptions are samples TZ13 and TZ10, where the concentrations in olivine are ~8%
279 lower than in pyroxene, and sample TZ15, where a difference of ~17% is observed. The latter
280 might be explained by an inaccurate magmatic He correction due to the high $^{4}He^{*}$ correction
281 estimated for this sample.
282 For those sites where two samples were taken from a single flow (TZ10 and TZ12 at 2740m;
283 TZ13 and TZ14 at 3050m) the $^{3}He_{cos}$ concentrations in pyroxenes differ by 10% (TZ10 and
284 TZ12) and 7% (TZ13 and TZ14) and in the olivines of TZ13 and TZ14 by 12%. The
285 concentrations in the olivines of TZ10 and TZ12 agree within analytical uncertainties (1σ).

286

287 - Fig. 2 about here -

288

289 Determination of cosmogenic ^{21}Ne concentrations

290 In young (< 500 ka) basalts concentrations of cosmogenic ^{21}Ne are calculated using:

291

292 $$^{21}Ne_{cos} = [(^{21}Ne/^{20}Ne)_m - (^{21}Ne/^{20}Ne)_{tr}] \times {}^{20}Ne_m \qquad \text{Eq. 2}$$

293

294 (Niedermann, 2002), where $^{21}Ne_{cos}$ is the cosmogenic ^{21}Ne concentration, $(^{21}Ne/^{20}Ne)_m$ and

295 $^{20}Ne_m$ are the measured Ne isotope ratio and concentration from melt extractions, and

296 $(^{21}Ne/^{20}Ne)_{tr}$ is the trapped ^{21}Ne/ ^{20}Ne value. Most subaerially erupted basalts have a trapped

297 Ne isotopic composition similar to that of atmospheric Ne (e.g. Dunai and Porcelli, 2002,

298 Althaus et al., 2003), with isotope ratios of ^{21}Ne/^{20}Ne = 0.00296 and ^{22}Ne/^{20}Ne = 0.1020

299 (Eberhardt et al., 1965). It is assumed in this calculation that the nucleogenic ^{21}Ne component

300 is insignificant.

301 Neon isotope data are presented in Table A4 and in Fig. 3. All isotope data have been

302 corrected for isobaric interferences, mass discrimination effects and analytical blanks (see

303 Appendix). Examination of neon measurements on a three-isotope plot enables assessment of

304 the neon inventory in a sample. In Fig. 3, olivine and pyroxene data are defined by a linear

305 regression line y = 1.0539x + 0.0994, which is the same, within error, as the spallation line for

306 pyroxenes ([1.069 ± 0.035]x + 0.099) reported by Schäfer et al. (1999). The regression line

307 passes through the air component and no nucleogenic or mantle component is identified in the

308 heating steps. This supports our assumption that the trapped component has an atmospheric

309 composition.

310 Concentrations of $^{21}Ne_{cos}$ range from (2.79 to 19.0) × 10^6 at g^{-1} in pyroxenes and from (24.8 to
311 34.9) × 10^6 at g^{-1} in olivines (Table 3). In the four samples containing cogenetic olivine and
312 pyroxene, $^{21}Ne_{cos}(px)/^{21}Ne_{cos}(ol)$ range from 0.50 to 0.54. These are indistinguishable from the
313 values predicted by modelling $^{21}Ne_{cos}$ production rates for the olivines (Fo_{81}) and pyroxenes
314 (En_{41-43}) in this study ($^{21}Ne_{cos}(px)/^{21}Ne_{cos}(ol)$ = 0.50 to 0.53) using major element compositions
315 determined by microprobe and the elemental production rates of Masarik (2002) (see Table
316 2c). Our values are also the same within analytical error as (i) a measured ratio of 0.49 ± 0.07,
317 deduced from the ^{21}Ne concentrations in cogenetic olivines (Fo_{82}) and pyroxenes (En_{44}) of
318 sample 250406-16 in Fenton et al. (2009), and (ii) a calculated ratio of 0.56 ± 0.18,
319 determined from experimentally calibrated ^{21}Ne production rate values for olivines and
320 pyroxenes ($P^{21}Ne_{cos}(Fo_{81})$ = 45 ± 4 atoms g^{-1} a^{-1}, Poreda and Cerling, 1992; $P^{21}Ne_{cos}(En_{43-44})$ =
321 25 ± 8 atoms g^{-1} a^{-1}, Fenton et al., 2009). The large uncertainty associated with the
322 experimental production rate ratio is mainly a function of the 32% uncertainty in the
323 independent lava-flow age determined in the study of Fenton et al. (2009). Despite the
324 differences in pyroxene composition among the samples and experimental production rates,
325 our mean value of 0.52 ± 0.02 thus seems a reasonable estimate of the relative production
326 ratio of ^{21}Ne in olivines (Fo_{81-82}) and pyroxenes (En_{41-44}).
327 Both olivine $^{21}Ne_{cos}$ concentrations and pyroxene $^{21}Ne_{cos}$ concentrations of samples TZ10 and
328 TZ12 (flow at 2740 m) agree within analytical error (1σ). Also, for the samples taken from
329 the flow at 3050 m (TZ13 and TZ14), the olivine $^{21}Ne_{cos}$ concentrations in the two samples are
330 identical within uncertainties, but the concentration of $^{21}Ne_{cos}$ in the pyroxenes is 12% higher
331 in TZ14 than in TZ13.
332
333 - Fig. 3 about here -
334

335 **3.4 Major and trace elements**

336 For the calculations of cosmogenic ^{36}Cl, chemical compositions of the mineral aliquots and of
337 bulk-rock were analyzed at the Service d'Analyse des Roches et des Minéraux du CNRS
338 (CRPG, Nancy, France). Major elements were determined by ICP-OES and trace elements by
339 ICP-MS, except Li (atomic absorption), B (colorimetry), H_2O (Karl Fischer titration) and Cl
340 (spectrophotometry). Bulk-rock concentrations of the major elements and of H, Li, B, Sm,
341 Gd, U, Th and Cl are given in Table A2. These are required for calculating low-energy
342 neutron distributions at the land/atmosphere interface. Aliquots of the etched mineral grains,
343 taken before their complete dissolution, represent the part of sample dissolved for ^{36}Cl
344 extraction and served for the analysis of the corresponding target element concentrations (Ca,
345 K, Ti and Fe). These concentrations (Table 2a) and the Cl concentrations, determined by
346 isotope dilution during AMS measurements (Table A1), were used to calculate ^{36}Cl
347 production from all production mechanisms in the dissolved samples.
348 U and Th concentrations in groundmass and phenocryst separates, required for calculation of
349 $^{4}He^{*}$ (as described in the previous section), were measured by ICP-MS at CRPG using the
350 procedure optimized for low abundances in (U-Th)/He dating (Carignan et al., 2001; Kraml et
351 al., 2006). Measured U and Th concentrations are listed in Table 2b (minerals) and Table A2
352 (groundmass). Li concentrations in the phenocrysts are required to estimate the cosmogenic
353 ^{3}He production from thermal and epithermal neutron capture on ^{6}Li. The concentrations were
354 measured at CRPG and are listed in Table 2b.
355 The compositions of chemically untreated olivine and pyroxene phenocrysts were determined
356 by electron microprobe at l'Université Henri Poincaré, Nancy (Table 2c) and served to assess
357 dependence of ^{21}Ne production on mineral composition (see previous section). Elemental
358 production rates estimated for ^{21}Ne by Masarik (2002) are also given in Table 2c.
359

- Table 2 about here –

- Table 3 about here -

4. Approaches to TCN cross-calibrations

A common approach for comparing different TCN production rates in the same sample is to calculate ratios of cosmogenic nuclide concentrations. This approach has previously been adopted for cross-calibration of ^{3}He and/or ^{21}Ne production rates with ^{10}Be (Gayer et al., 2004, Kober et al., 2005, Farley et al., 2006, Amidon et al., 2008, Amidon et al., 2009), and for evaluation of relative ^{3}He and ^{21}Ne production rates (Fenton et al., 2009). When cross-calibrating TCN in several samples along an altitude transect, an increasing or decreasing trend versus altitude would indicate that the nuclides have different altitude dependences (Gayer et al., 2004, Amidon et al., 2008).

In these studies, the compared nuclides are primarily produced by spallation reactions. In the case of the noble gases ^{3}He and ^{21}Ne, trapped nucleogenic and radiogenic contributions were subtracted prior to cross-calibration, so that only cosmogenic components were taken into account. Predominantly spallation-produced nuclides such as ^{3}He, ^{21}Ne and ^{10}Be should accumulate in a given sample with a constant ratio. However, despite the fact that these nuclides are predominantly spallogenic in origin, there are nevertheless variations in production rate related to the chemical composition of the mineral involved.

1) Cosmogenic production of ^{3}He by thermal neutron capture on ^{6}Li has been shown to be potentially significant in Li-rich minerals and rocks (Dunai et al., 2007) and may require a correction. This approach has not been done in the pioneer paper of Gayer et al. (2004) but has since been addressed (e.g. Amidon et al., 2009). However, Li concentrations in mafic

minerals such as olivine and pyroxenes are generally low (< 10 ppm). In this study Li concentrations range between 2 and 7 ppm (Table 2b) and thus contribute less than 1% to the ^{3}He budget.

2) Even though ^{3}He and ^{21}Ne are commonly calibrated for a given mineral phase, their production rates also depend on the mineral chemical composition (e.g. Masarik and Reedy, 1996). ^{3}He is mainly produced from O and Si, as well as from Mg, Fe, Al and Ca, with relatively uniform elemental production rates. In contrast, ^{21}Ne is not produced from O, but from Na, Mg, Al, Si, Ca and Fe with significant variations between elemental production rates (e.g. Masarik and Reedy, 1996, Masarik, 2002, see Table 2c). The production rate of ^{21}Ne is therefore more sensitive than that of ^{3}He to variations in mineral composition. As a consequence, if the composition of a mineral phase varies significantly within the sample set, ^{3}He/^{21}Ne ratios may also vary significantly.

While relative ^{3}He, ^{21}Ne and ^{10}Be production rates are only slightly dependent on mineral chemistry, the situation is significantly more complex for ^{36}Cl. In order to compare spallogenic nuclides with ^{36}Cl, three issues have to be considered.

i) Mineral composition is more important when comparing cosmogenic noble gas concentrations to those of ^{36}Cl. ^{36}Cl is produced from fewer target elements than ^{3}He and ^{21}Ne, dominantly from Ca, K and ^{35}Cl (review in Schimmelpfennig et al., 2009), making its production rate extremely sensitive to the mineral composition.

ii) The noble gases ^{3}He and ^{21}Ne are stable TCN, while ^{10}Be and ^{36}Cl are radioactive. Concentration ratios of a stable and a radioactive nuclide will not remain constant over long exposure durations due to decay of the radionuclide. In the case of ^{10}Be, which has a half-life of 1.39 Ma (Chmeleff et al., 2010, Korschinek et al., 2010), this becomes significant for exposure ages longer than 100 ka, while in the case of the shorter-lived ^{36}Cl (half-life 301 ka),

410 the effect is significant for even shorter exposure durations. In addition, the effect depends on
411 erosion (Goethals et al., 2009), whereas the stable nuclides (^{3}He, ^{21}Ne) accumulate with a
412 constant ratio, irrespective of erosion rate. For example, the concentration ratio of ^{36}Cl/^{3}He or
413 ^{36}Cl/^{21}Ne is approximately 12% smaller than their production ratio for a 100 ka old surface
414 eroding at <1 m/Ma; at lower ages or higher erosion rates the difference becomes smaller
415 (according to Goethals et al., 2009; the muogenic ^{36}Cl contribution is neglected here).
416 Therefore, radioactive decay should be taken into account when comparing TCN
417 concentrations, especially if the samples have a range of exposure ages as they do in this
418 study.
419 iii) Cosmogenic ^{36}Cl is not only produced by spallation. A significant ^{36}Cl contribution is also
420 derived from slow negative-muon capture by Ca, and to a lesser degree by K (review in
421 Schimmelpfennig et al., 2009). Because the altitude-dependence of the muon flux is weaker
422 than that of the fast neutrons (e.g. Stone, 2000), with increasing altitude the production of ^{36}Cl
423 by spallation increases at a higher rate than ^{36}Cl production by muon-capture. Hence, over a
424 given altitude transect, total ^{36}Cl production will not be proportional to the production of TCN
425 derived almost purely from spallation. ^{36}Cl is also produced by thermal and epithermal
426 neutron capture on the trace element ^{35}Cl, and a significant proportion of ^{36}Cl can result from a
427 high level of Cl (>50 ppm) in a sample (Schimmelpfennig et al., 2009). However, as for ^{3}He
428 production due to ^{6}Li, when Cl concentrations in a sample are low (a few ppm) this
429 mechanism contributes generally insignificantly to the ^{36}Cl production. Variations in ^{36}Cl
430 concentrations in samples of the same lithology might therefore be a consequence of varying
431 Cl concentrations.
432
433

4.1 Comparing cosmogenic ^{36}Cl, ^{3}He and ^{21}Ne concentrations

Because of the favourable chemical composition of the pyroxene phenocrysts in our samples (notably low Cl, low K concentrations and similar Ca concentrations) we first directly compare the ratios of the cosmogenic ^{36}Cl, ^{3}He and ^{21}Ne concentrations (Fig. 4), ignoring the effects of radioactive decay, erosion and muogenic ^{36}Cl contribution. The ^{36}Cl contribution from Ca spallation is maximized by extraction from the Cl-poor, Ca-rich pyroxenes (max. 10 ppm Cl, see Table A1). Hence, spallation of Ca contributes between 86% and 90% of ^{36}Cl in these samples, while the contribution from spallation of K is < 1% and that from spallation of Ti and Fe together is about 3% (calculated using the ^{36}Cl calculation spreadsheet published in Schimmelpfennig et al., 2009). The contributions from thermal and epithermal neutron capture on ^{6}Li and ^{35}Cl, respectively, are < 1% for ^{3}He and 3.7% or less for ^{36}Cl. The Li-derived ^{3}He contribution is based on Li concentrations measured in the minerals, Table 2b, and calculated using a version of CHLOE (Phillips and Plummer, 1996) modified for ^{3}He production (R. Pik and P. Burnard, unpublished). The ^{36}Cl contributions due to slow negative-muon capture are 10% at 1000 m altitude and decrease to 5% at 4300 m. As a consequence we might expect a slight overestimate of the ^{36}Cl to noble gas nuclide ratios at low altitudes relative to high altitudes due to the muogenic ^{36}Cl contribution.

Since, to our knowledge, ^{36}Cl has never been measured in pyroxene before, we validate this method by measuring ^{36}Cl in co-genetic plagioclases in sample TZ15. Feldspar is an accepted ^{36}Cl target mineral (Stone et al., 1996, Evans et al. 1997, Schimmelpfennig et al. 2009). The ^{36}Cl concentrations in both mineral phases of TZ15 are given in Table A1 in the Appendix. Since the Ca concentrations are higher in the pyroxene by almost a factor of two and also the K and Cl concentrations differ between both mineral phases, ^{36}Cl concentrations cannot be directly compared. We therefore calculated the apparent exposure ages from these two minerals using the ^{36}Cl calculation spreadsheet (Schimmelpfennig et al., 2009) and the SLHL

458 production rate for spallation of Ca by Stone et al. (1996), which yields 14.4 ± 1.1 ka for
459 pyroxene and 14.3 ± 1.1 ka for plagioclase, confirming that pyroxene is a suitable mineral for
460 ^{36}Cl surface exposure age determinations.
461 Fig. 4 shows the ratios of the cosmogenic nuclide concentrations versus altitude. In pyroxene,
462 the mean values of the ratios and their standard deviations are 0.0582 ± 0.0061 (n=8) for
463 ^{36}Cl/^{3}He, 0.1864 ± 0.0085 (n=6) for ^{21}Ne/^{3}He and 0.301 ± 0.020 (n=6) for ^{36}Cl/^{21}Ne. For each
464 of the three TCN ratios, all individual measurements, except the ^{36}Cl/^{3}He ratio of TZ15, lie
465 within the standard deviation of the respective mean values and therefore do not show any
466 altitudinal dependence. It should be noted that TCN concentration ratios are composition-
467 dependent, particularly when ^{36}Cl and ^{21}Ne are involved, and they should not be expected to
468 be the same in different mineral phases or in pyroxenes with significantly different
469 compositions. In this study, the compositions of the pyroxene minerals are very similar, only
470 TZ09 (En_{45}) and TZ15 (En_{44}) diverge slightly from the other samples (En_{41-43}). Significant
471 differences are observed in the Ca, Fe and Al concentrations (Table 2), each of them being an
472 important target element for at least one of the TCN in this study. Theoretical calculations of
473 mineral production rates, based on these compositions and on the elemental production rates
474 by Masarik (2002), predict that the ^{36}Cl/^{3}He and ^{36}Cl/^{21}Ne ratios of these two samples should
475 be about 10% to 15% lower than those of the other samples.
476 ^{21}Ne/^{3}He was also determined in olivine from four of the samples: TZ10 and TZ12 from the
477 2740 m sample site and TZ13 and TZ14 from the 3000 m site (Table 3b, Fig. 4b). At higher
478 altitudes, only ^{3}He could be determined in olivines. ^{36}Cl could not be measured in olivine
479 since this mineral contains no abundant target element for production of this nuclide. A mean
480 ^{21}Ne/^{3}He value of 0.377 ± 0.018 was determined and all four measurements lie within the
481 standard deviation of the mean value. No variation is observed between the two sample
482 locations.

- Fig. 4 about here -

4.2 Comparing apparent ^{36}Cl, ^{3}He and ^{21}Ne exposure ages

If erosion is negligible, samples collected from a single lava-flow or glacially created surface should yield the same exposure age irrespective of TCN or mineral phase. All composition-, production pathway- and decay-related differences between the nuclides should be accounted for in the exposure age calculation. Errors in scaling factors for spallation reactions will cancel out provided the same scaling method is applicable for all reactions. A separate scaling factor is required for production of ^{36}Cl from muons. However, errors in the muon scaling factor are expected to have only a minor influence on calculated exposure age ratios, because ^{36}Cl contributions from muons are not higher than 5-10%. We choose the scaling method of Stone (2000), because all the SLHL production rates considered below were originally scaled according to either Stone (2000) or to Lal (1991); these two methods are equivalent to each other. The applied scaling factors are listed in Table 1.

The selection of SLHL production rates poses a more serious challenge, because for each nuclide several experimentally calibrated and modelled production rates exist, covering a quite large range of values. We will limit our study to select a single SLHL production rate for each nuclide. If the SLHL production rates of all nuclides were perfectly known and all nuclides were equally altitude-dependent, the exposure age ratios should be equal to 1 (cf. Fig. 5). Systematic discrepancies would indicate that one or both SLHL production rates are inaccurate. Without an independent age control it is, however, not possible to determine which production rate is correct.

For ^{36}Cl, production rates are not mineral- but target-element-specific. Spallation of Ca is the most important production mechanism in our pyroxenes. We use the production rate for

508 spallation of Ca with a value of 48.8 ± 1.7 atoms (g Ca)$^{-1}$ a^{-1} (Stone et al., 1996). For ^{3}He, we
509 use the production rate of 128 ± 5 atoms (g mineral)$^{-1}$ a^{-1} (Blard et al., 2006). This production
510 rate is assumed to be valid for pyroxene as well as olivine because cosmogenic ^{3}He
511 concentrations are identical within analytical uncertainty in the cogenetic olivines and
512 pyroxenes of our study (Fig. 2). For ^{21}Ne, both modelled elemental production rates and
513 experimentally calibrated mineral-specific production rates are available. Here, we use the
514 calibrated SLHL production rate of 25 ± 8 atoms (g pyroxene)$^{-1}$ a^{-1} of Fenton et al. (2009).
515 The compositions of pyroxenes in Fenton et al. (2009) (En_{43-44}) fall within the range of those
516 in our study (En_{41-45}).
517 The resulting apparent exposure ages range between 14 ka and 170 ka (Table 4). For each
518 nuclide pair, the exposure age ratios are then calculated. These are plotted as a function of
519 altitude in Fig. 5. This graph shows a similar pattern to the concentration plot, indicating that
520 the radioactive decay of ^{36}Cl (as can be expected for relatively young exposure ages),
521 differences in mineral composition and the ^{36}Cl production by slow muon capture have only a
522 minor impact on the altitudinal trend of these data.
523 Despite this overall similarity, exposure age ratios appear to exhibit a slight dependence on
524 altitude. Notably ^{36}Cl/^{3}He decreases with altitude; this trend is essentially defined by samples
525 TZ09 (1000 m) and TZ15 (4100 m), with 30% difference between these two samples without
526 overlap of the estimated uncertainties. However, the TZ15 ^{36}Cl/^{21}Ne age ratio is
527 indistinguishable from those at lower altitudes. An error in the calculation of the ^{3}He age of
528 TZ15 is therefore possible. Since TZ15 was taken from a polished glacial surface of an old
529 dyke (see section 2, formation age >> exposure age), it is subject to an uncertain correction
530 for radiogenic ^{4}He*, which affects the cosmogenic ^{3}He concentration estimation (section 3.3).
531 The black circles at the altitude of TZ15 in Fig. 5a and b represent the age ratios when
532 assuming the highest correction for radiogenic ^{4}He* based on measured U and Th

concentrations, the $^{40}Ar/^{39}Ar$ age and the minimum grain size of the phenocrysts (2 mm). The open circles mark the ratios if no such correction is done, thus indicating the trend towards higher ratios if the radiogenic $^{4}He^{*}$ correction was overestimated. Furthermore, the surface of the TZ09 flow was clearly eroded. Erosion can have an effect on ratios involving ^{36}Cl, because it has a shorter half-life than the other nuclides and because the ^{36}Cl contribution from slow negative-muon capture is less dependent on erosion than the ^{36}Cl contribution from spallation due to the longer attenuation length of the muons. Consequently, if erosion is not taken into account then the calculated apparent ^{36}Cl exposure age is higher relative to the calculated apparent ^{3}He exposure age. The ratio of the apparent exposure ages of TZ09 is displayed in Fig. 5a by the black circle, while the open diamond represents the ratio if erosion is taken into account. For this calculation we assumed an eroded rock layer of 30 cm, which corresponds to the estimated maximum erosion based on field evidence.

When these considerations are taken into account all exposure age ratios overlap within their uncertainties over the examined altitude range. No clear altitudinal variation in nuclide production can be demonstrated without ambiguity, regardless of the production rate or nuclide pair examined. Also, no correlation of the ratios with the different exposure durations of the surfaces can be observed.

At present, accurate independent age constraints are not available for the sampled lava flows, preventing us from evaluating SLHL production rates. The production rates chosen here result in exposure ages that mostly agree between all three nuclides (Table 4), i.e. the exposure age ratios presented in Fig. 5 are generally equal to 1. But it is important to stress that this would also have been the case if for all three nuclides accordingly lower or higher SLHL production rates had been chosen and that this does not affect the evaluation of the altitude dependence of the relative nuclide production rates.

- Table 4 -

- Fig. 5 about here -

5. Comparison with other cross-calibrations

A significant altitudinal variation of the relative production rates of ^{3}He compared to other nuclides, as was proposed by Gayer et al. (2004) and Amidon et al. (2008), is not documented by the Kilimanjaro data set. Even though the altitude range of samples TZ10 to TZ19 is similar to that of the Himalayan samples (3000 - 4600 m in Gayer et al., 2004, and 3200 - 4800 m in Amidon et al., 2008) and Amidon et al. (2008) documented an increase in the ^{3}He/^{10}Be concentration ratio of up to 40% for their transect, all exposure age ratios in our study agree at the 1σ level for the corresponding altitude range (2700 - 4300 m) (Fig. 5). Regarding only the nominal values of the ^{36}Cl/^{3}He exposure age ratios over the whole altitude range in our study (1000 – 4300 m), i.e. ignoring the overlapping uncertainties, results in a 17% increase. However, this variation is much less than that documented for the Himalayan transects (Fig. 6). Possible explanations could be that i) no significant differences in relative production rates exist and the anomaly in the nuclide ratios of the Himalayan samples is due to factors other than changes in the nucleon energy spectrum; ii) the altitude dependences of ^{36}Cl, ^{21}Ne and ^{3}He production are more similar than for ^{10}Be and ^{3}He; or iii) a latitude effect must be considered, since the Himalaya sites are at higher latitudes (27-28°N) than Mt. Kilimanjaro (3°S). Due to the decreasing shielding effect of the geomagnetic field with increasing latitude, the cosmic ray flux becomes stronger. As a consequence, the flux at 4000 m altitude and a latitude of 30° is about 35% higher than at the same altitude and a latitude of 3° (according to the scaling method by Stone, 2000). Also, at high latitudes the energy

583 spectrum of the flux becomes on average less energetic (Gosse and Phillips, 2001). This could
584 explain different altitude dependences of the relative production rates, even though the
585 altitudes are very similar for all studies considered here. However, the possibility of such a
586 latitude effect has to be further investigated.
587 The mean values of the $^{21}Ne/^{3}He$ concentration ratios in pyroxene (0.1864 ± 0.0085) and
588 olivine (0.377 ± 0.018) are slightly lower but in agreement within 1σ with those of a number
589 of studies undertaken at mid latitudes and altitudes between 1000 and 2000 m, e.g. Fenton et
590 al. (2009) (0.204 ± 0.014 in pyroxene and 0.400 ± 0.029 in olivine), Poreda and Cerling
591 (1992) (0.41 ± 0.05 in olivine) and Kounov et al. (2007) (0.225 ± 0.027 in pyroxene),
592 suggesting that the production rates of ^{3}He and ^{21}Ne in these minerals have the same altitude
593 and latitude dependences. However, two studies from Antarctica reported significantly higher
594 $^{21}Ne/^{3}He$ ratios in pyroxene from altitudes around 1000 – 2000 m (0.22-0.26 in Bruno et al.,
595 1997; 0.21 - 0.26 in Schäfer et al., 1999). The compositions of their pyroxenes are
596 significantly different from those in our study, but theoretical calculations based on these
597 compositions and the elemental production rates of Masarik (2002) predict $^{21}Ne/^{3}He$ ratios
598 lower than those in our study. The compositional differences cannot therefore explain the
599 discrepancy in the ratios. Other possible explanations are (i) the latitude effect proposed
600 before, suggesting that the production rate of ^{21}Ne increases at a higher rate than that of ^{3}He
601 with increasing latitude, or (ii) significant fractions of plagioclase and quartz in the Antarctic
602 pyroxene separates, as suggested by Niedermann et al. (2007). The presence of plagioclase
603 and quartz would lower the ^{3}He concentration, because these minerals are less retentive for
604 Helium than pyroxene. Several studies (Margerison et al., 2005, Niedermann et al., 2007,
605 Oberholzer et al., 2008) reported difficulties in obtaining pure pyroxene separates from the
606 sampled Antarctic dolerite, and $^{21}Ne/^{3}He$ ratios of four pure pyroxene separates re-measured

607 from the sample suite of Schäfer et al. (1999) are indeed lower (0.181-0.217, Niedermann et
608 al., 2007) than in the earlier study.
609 Staudacher and Allègre (1993) measured significantly lower $^{21}Ne/^{3}He$ ratios in olivine (0.23 -
610 0.30) at latitude 21°S and altitudes around 2300 m. Neither the mineral compositions, which
611 are very similar in their and our study, nor the hypothesized latitude effect seem likely to
612 explain this discrepancy. Assumedly, the calculations of their cosmogenic noble gas
613 concentrations were subject to inaccurate correction for non-cosmogenic components.
614 To our knowledge, Licciardi et al. (2008) is the only study in which ^{36}Cl has been co-
615 calibrated with another nuclide, ^{3}He. ^{36}Cl was measured in basaltic whole rock, while ^{3}He was
616 determined in olivine phenocrysts of the same samples (Licciardi et al., 2006). However, a
617 comparison between the relative production rates of ^{36}Cl and ^{3}He in their study and ours
618 cannot be performed for several reasons. ^{36}Cl concentrations are not given in Licciardi et al.
619 (2008). Also, the basalts have varying Cl concentrations (up to 61 ppm), which result in ^{36}Cl
620 contributions from capture of low-energy neutrons on ^{35}Cl of up to 26%, so that $^{36}Cl/^{3}He$
621 concentration ratios could not be expected to be constant from sample to sample. Finally, all
622 samples come from a narrow range of altitudes (20-460 m) excluding altitude dependent
623 comparisons.
624
625 - Fig. 6 about here -
626
627 **6. Conclusions**
628 This is the first study that deals with the cross-calibration of three cosmogenic nuclides (^{36}Cl,
629 ^{3}He and ^{21}Ne) in minerals over a large altitudinal profile (1000 - 4300 m) at low latitude (3°
630 S). All three nuclides have been measured in pyroxene phenocrysts, and ^{3}He and ^{21}Ne have
631 additionally been measured in olivine at two elevations. ^{36}Cl has also been determined in

plagioclase co-existing with pyroxene in one of the samples. Calculated exposure ages from both minerals yield the same result confirming the reliability of ^{36}Cl measurements in pyroxene.

Cosmogenic ^{21}Ne/^{3}He concentration ratios in pyroxene are 0.1864 ± 0.0085 and those in olivine are 0.377 ± 0.018, agreeing with previously determined ratios of these nuclides (Poreda and Cerling, 1992, Kounov et al., 2007, Fenton et al., 2009). In our samples, the ^{36}Cl/^{3}He and ^{36}Cl/^{21}Ne concentration ratios are 0.0582 ± 0.0061 and 0.301 ± 0.020, respectively. These concentration ratios can be very different between samples, since the ^{36}Cl production rate in a mineral depends strongly on the target element concentrations.

No significant altitude dependence of the relative production of any of the nuclides can be observed, in contrast to altitude-dependent variations documented in previous studies (Gayer et al., 2004, Amidon et al., 2008). Our observation is based on nuclide concentration ratios and calculated apparent exposure age ratios plotted versus the elevations of the sample sites. This suggests that production rates of the investigated nuclides are proportional to each other between mid and high altitudes at low latitude, implying that no nuclide-specific scaling factors are needed at this site. However, the latitude effect for cross-calibrations has to be further evaluated.

Although independently determined ages for the studied lava surfaces are not available at present, the consistency in the data-set should enable progress to be made in the determination of the production rates of all three nuclides as soon as the production rate of one of the nuclides has been accurately defined.

Acknowledgements:

F. Palhol and B. Marty are thanked for assistance in the field. This research would never have been possible without the enormous help from the University of Dar es Salaam, TANAPA, and Kilimanjaro National Park in Tanzania. We would particularly like to mention Dr. J. Wakibara (TANAPA), Fred Mangasini (University of Dar es Salaam) and Chamba Makene (Geological Survey of Tanzania), as well as Kilimanjaro guides R. Mtui and Zakaria and their team of porters at Marangu. Back in the laboratories, thanks goes to E. Davy for sample preparation, E. Schnabel for measurements at GFZ, B. Tibari and L. Zimmermann for help at CRPG, T. Guilderson and T. Brown as well as all the staff of the CAMS-LLNL for ^{36}Cl measurements and J. Wijbrans at Vrije Universiteit, Amsterdam, for $^{40}Ar/^{39}Ar$ analyses and discussion. Finally, David Shuster and an anonymous reviewer are gratefully acknowledged for their thorough and very constructive reviews that greatly improved the manuscript. This project was conducted as part of the CRONUS-EU Research Training Network (EU FP6 Marie Curie Actions, project 511927).

References:

Althaus, T., Niedermann, S., Erzinger, J., 2003. Noble gases in olivine phenocrysts from drill core samples of the Hawaii Scientific Drilling Project (HSDP) pilot and main holes (Mauna Loa and Mauna Kea, Hawaii). Geochemistry Geophysics Geosystems 4, 8701, doi: 10.1029/2001GC000275.

Amidon, W., Farley, K., Burbank, D., Prattsitaula, B., 2008. Anomalous cosmogenic ^{3}He production and elevation scaling in the high Himalaya. Earth and Planetary Science Letters 265 (1-2), 287-301.

Amidon, W. H., Rood, D. H., Farley, K. A., 2009. Cosmogenic ^{3}He and ^{21}Ne production rates calibrated against ^{10}Be in minerals from the Coso volcanic field. Earth and Planetary Science Letters 280 (1-4), 194-204.

Balco, G., Shuster, D. L., 2009. Production rate of cosmogenic ^{21}Ne in quartz estimated from ^{10}Be, ^{26}Al, and ^{21}Ne concentrations in slowly eroding Antarctic bedrock surfaces. Earth and Planetary Science Letters 281 (1-2), 48-58.

Balco, G., Stone, J., Lifton, N., Dunai, T., 2008. A complete and easily accessible means of calculating surface exposure ages or erosion rates from ^{10}Be and ^{26}Al measurements. Quaternary Geochronology 3 (3), 174-195.

Balco, G., Briner, J., Finkel, R. C., Rayburn, J. A., Ridge, J. C., Schaefer, J. M., 2009. Regional beryllium-10 production rate calibration for late-glacial northeastern North America. Quaternary Geochronology 4 (2), 93-107.

Blard, P. H., Farley, K. A., 2008. The influence of radiogenic ^{4}He on cosmogenic ^{3}He determinations in volcanic olivine and pyroxene. Earth and Planetary Science Letters 276 (1-2), 20-29.

Blard, P. H., Pik, R., 2008. An alternative isochron method for measuring cosmogenic ^{3}He in lava flows. Chemical Geology 251, 20-32.

Blard, P. H., Lavé, J., Pik, R., Quidelleur, X., Bourlés, D., Kieffer, G., 2005. Fossil cosmogenic ^{3}He record from K-Ar dated basaltic flows of Mount Etna volcano (Sicily, 38°N): Evaluation of a new paleoaltimeter. Earth and Planetary Science Letters 236, 613-631.

Blard, P. H., Pik, R., Lavé, J., Bourlès, D. L., Burnard, P., Yokochi, R., Marty, B., Trusdell, F., 2006. Cosmogenic ^{3}He production rates revisited from evidences of grain size dependent release of matrix-sited helium. Earth and Planetary Science Letters 247 (3-4), 222-234.

Bruno, L.A., Baur, H., Graf, T., Schlüchter, C., Signer, P., Wieler, R., 1997. Dating of Sirius Group Tillites in the Antarctic Dry Valleys with cosmogenic ^{3}He and ^{21}Ne. Earth and Planetary Science Letters 147, 37–54.

710 Carignan, J., Hild, P., Mevelle, G., Morel, J., Yeghicheyan, D., 2001. Routine analyses of trace elements in
711 geological samples using flow injection and low pressure on-line liquid chromatography coupled to ICP-MS; a
712 study of geochemical reference materials BR, DR-N, UB-N, AN-G and GH. Geostandards Newsletter 25, 187-
713 198.
714
715 Cerling, T. E., Craig, H., 1994. Cosmogenic ^{3}He production rates from 39°N to 46°N latitude, western USA and
716 France. Geochimica et Cosmochimica Acta 58, 249-255.
717
718 Chmeleff, J., von Blanckenburg, F., Kossert, K., Jakob, D., 2010. Determination of the ^{10}Be half-life by
719 multicollector ICP-MS and liquid scintillation counting. Nuclear Instruments and Methods in Physics Research
720 Section B 268, 192-199.
721
722 Desilets, D., Zreda, M., 2003. Spatial and temporal distribution of secondary cosmic-ray nucleon intensities and
723 applications to in situ cosmogenic dating. Earth and Planetary Science Letters 206, 21-42.
724
725 Desilets, D., Zreda, M., Prabu, T., 2006. Extended scaling factors for in situ cosmogenic nuclides: New
726 measurements at low latitude. Earth and Planetary Science Letters 246 (3- 4), 265-276.
727
728 Downie, C., Wilkinson, P., 1972. The Geology of Kilimanjaro. The Department of Geology, The University of
729 Sheffield, Sheffield, 253 pp.
730
731 Dunai T. J., 2001a. Influence of secular variation of the geomagnetic field on production rates of in situ produced
732 cosmogenic nuclides. Earth and Planetary Science Letters 193, 197-212.
733
734 Dunai T.J, 2001b. Reply to comment on 'Scaling factors for production rates of in situ produced cosmogenic
735 nuclides: a critical reevaluation' by Darin Desilets, Marek Zreda and Nathaniel Lifton. Earth and Planetary
736 Science Letters 188, 289-298.
737
738 Dunai T.J., Wijbrans, J.R., 2000. Long-term cosmogenic ^{3}He production rates (152 ka-1.35 Ma) from ^{40}Ar/^{39}Ar
739 dated basalt flows at 29°N latitude. Earth and Planetary Science Letters 176, 147-156.

740

741 Dunai, T.J., Porcelli, D., 2002. Storage and transport of noble gases in the subcontinental lithosphere. Reviews in
742 Mineralogy and Geochemistry 47, 371-409.
743
744 Dunai, T. J., Stuart, F. M., Pik, R., Burnard, P., Gayer, E., 2007. Production of ^{3}He in crustal rocks by
745 cosmogenic thermal neutrons. Earth and Planetary Science Letters 258 (1-2), 228-236.
746
747 Eberhardt, P., Eugster, O., Marti, K., 1965. A redetermination of the isotopic composition of atmospheric neon.
748 Zeitschrift für Naturforschung 20a, 623-624.
749
750 Evans, J. M., Stone, J. O., Fifield, L. K., Cresswell, R. G., 1997. Cosmogenic ^{36}Cl production in K-feldspar.
751 Nuclear Instruments and Methods in Physics Research Section B 123, 334-340.
752
753 Farley, K. A., Libarkin, J., Mukhopadhyay, S., Amidon, W., 2006. Cosmogenic and nucleogenic ^{3}He in apatite,
754 titanite, and zircon. Earth and Planetary Science Letters 248 (1-2), 451-461.
755
756 Fenton, C. R., Niedermann, S., Goethals, M. M., Schneider, B., Wijbrans, J., 2009. Evaluation of cosmogenic
757 ^{3}He and ^{21}Ne production rates in olivine and pyroxene from two Pleistocene basalt flows, western Grand Canyon,
758 AZ, USA. Quaternary Geochronology 4, 475-492.
759
760 Gayer, E., Pik, R., Lavé, J., France-Lanord, C., Bourlès, D., Marty, B., 2004. Cosmogenic ^{3}He in Himalayan
761 garnets indicating an altitude dependence of the ^{3}He/^{10}Be production ratio. Earth and Planetary Science Letters
762 229 (1-2), 91-104.
763
764 Goethals, M. M., Hetzel, R., Niedermann, S., Wittmann, H., Fenton, C. R., Kubik, P. W., Christl, M., von
765 Blanckenburg, F., 2009. An improved experimental determination of cosmogenic ^{10}Be/^{21}Ne and ^{26}Al/^{21}Ne
766 production ratios in quartz. Earth and Planetary Science Letters 284, 187-198.
767
768 Gosse, J. C., Phillips, F. M., 2001. Terrestrial in situ cosmogenic nuclides: theory and application. Quaternary
769 Science Reviews 20, 1475-1560.

Kober, F., Ivy-Ochs, S., Leya, I., Baur, H., Magna, T., Wieler, R., Kubik, P. W., 2005. In situ cosmogenic ^{10}Be and ^{21}Ne in sanidine and in situ cosmogenic ^{3}He in Fe-Ti-oxide minerals. Earth and Planetary Science Letters 236 (1-2), 404-418.

Korschinek, G., Bergmaier, A., Faestermann, T., Gerstmann, U. C., Knie, K., Rugel, G., Wallner, A., Dillmann, I., Dollinger, G., Lierse von Gostomski, C., Kossert, K., Maiti, M., Poutivtsev, M., Remmert, A., 2010. A new value for the half-life of ^{10}Be by Heavy-Ion Elastic Recoil Detection and liquid scintillation counting. Nuclear Instruments and Methods in Physics Research Section B 268, 187-191.

Kounov, A., Niedermann, S., de Wit, M. J., Viola, G., Andreoli, M., Erzinger, J. (2007). Present denudation rates at selected sections of the South African escarpment and the elevated continental interior based on cosmogenic ^{3}He and ^{21}Ne. South African Journal of Geology 110, 235-248.

Kraml, M., Pik, R., Rahn, M., Carignan, J., Keller, J., 2006. A potential single grain ^{40}Ar/^{39}Ar, (U-Th)/He and FT age standard: the Limberg t3 tuff. Geostandards and Geoanalytical Research 30, 73-86.

Kurz, M. D., 1986. In situ production of terrestrial cosmogenic helium and some applications to geochronology. Geochimica et Cosmochimica Acta 50, 2855-2862.

Lal, D., 1991. Cosmic ray labeling of erosion surfaces: in situ nuclide production rates and erosion models. Earth and Planetary Science Letters 104, 424-439.

Licciardi, J., Kurz, M., Curtice, J., 2006. Cosmogenic ^{3}He production rates from Holocene lava flows in Iceland. Earth and Planetary Science Letters 246 (3-4), 251-264.

Licciardi, J., Denoncourt, C., Finkel, R., 2008. Cosmogenic ^{36}Cl production rates from Ca spallation in Iceland. Earth and Planetary Science Letters 267 (1-2), 365-377.

Lifton, N., Bieber, J., Clem, J., Duldig, M., Evenson, P., Humble, J., Pyle, R., 2005. Addressing solar modulation and long-term uncertainties in scaling secondary cosmic rays for in situ cosmogenic nuclide applications. Earth and Planetary Science Letters 239, 140-161.

Margerison, H. R., Phillips, W. M., Stuart, F. M., Sugden, D. E., 2005. Cosmogenic ^{3}He concentrations in ancient flood deposits from the Coombs Hills, northern Dry Valleys, East Antarctica: interpreting exposure ages and erosion rates. Earth and Planetary Science Letters 230, 163-175.

Masarik, J., 2002. Numerical simulation of in-situ production of cosmogenic nuclides. Geochimica et Cosmochimica Acta 66 (S1), Goldschmidt Conference Abstract A491.

Masarik, J., Reedy, R. C., 1996. Monte Carlo simulation of in-situ-produced cosmogenic nuclides. Radiocarbon 38, 163-164.

Niedermann, S., 2002. Cosmic-ray-produced noble gases in terrestrial rocks: Dating tools for surface processes. Reviews in Mineralogy and Geochemistry 47, 731-784.

Niedermann, S., Goethals, M. M., Pilz, P., 2009. Evidence for a high ^{3}He or low ^{10}Be production rate from cosmogenic nuclide cross-calibration. Geochimica et Cosmochimica Acta 73 (13, Suppl. 1), Goldschmidt Conference Abstract A940.

Niedermann, S., Schaefer, J. M., Wieler, R., Naumann, R., 2007. The production rate of cosmogenic 38Ar from calcium in terrestrial pyroxene. Earth and Planetary Science Letter 257, 596–608.

Nonnotte, P., Guillou, H., Gall, B. L., Benoit, M., Cotten, J., Scaillet, S., 2008. New K-Ar age determinations of Kilimanjaro volcano in the North Tanzanian diverging rift, East Africa. Journal of Volcanology and Geothermal Research 173 (1-2), 99-112.

Oberholzer, P., Baronik, C., Salvatore, M.C., Baur, H., Wieler, R., 2008. Dating late-Cenozoic erosional surfaces in Victoria Land, Antarctica, with cosmogenic neon in pyroxene. Antarctic Science 20, 89-98.

Phillips, F. M., Plummer, M. A., 1996. CHLOE: A program for interpreting in-situ cosmogenic nuclide data for surface exposure dating and erosion studies. Abstracts of the 7th international conference on Accelerator Mass Spectrometry, 98-99.

Poreda, R. J., Cerling, T. E., 1992. Cosmogenic neon in recent lavas from the western United States. Geophysical Research Letters 19, 1863-1866.

Schäfer, J. M., Ivy-Ochs, S., Wieler, R., Leya, I., Baur, H., Denton, G. H., Schlüchter, C., 1999. Cosmogenic noble gas studies in the oldest landscape on earth: surface exposure ages of the Dry Valleys, Antarctica. Earth and Planetary Science Letters 167 (3-4), 215-226.

Schimmelpfennig, I., Benedetti, L., Finkel, R., Pik, R., Blard, P. H., Bourlès, D., Burnard, P., Williams, A., 2009. Sources of in-situ ^{36}Cl in basaltic rocks. Implications for calibration of production rates. Quaternary Geochronology 4, 441-461.

Schimmelpfennig, I., Benedetti, L., Garreta, V., Pik, R., Blard, P. H., Burnard, P., Bourlès, D., Finkel, R., Ammon, K., Dunai, T., 2011. Calibration of cosmogenic ^{36}Cl production rates from Ca and K spallation in lava flows from Mt. Etna (38°N, Italy) and Payun Matru (36°S, Argentina). Geochimica et Cosmochimica Acta 75, 2611-2632.

Shanahan, T. M., Zreda, M., 2000. Chronology of Quaternary glaciations in East Africa. Earth and Planetary Science Letters 177 (1-2), 23-42.

Sharma, P., Kubik, P. W., Fehn, U., Gove, H. E., Nishiizumi, K., Elmore, D., 1990. Development of ^{36}Cl standards for AMS. Nuclear Instruments and Methods in Physics Research Section B 52, 410-415.

Staudacher, T., Allègre, C.J., 1993. The cosmic ray produced ^{3}He/^{21}Ne ratio in ultramafic rocks. Geophysical Research Letters, 20, 1075-1078.

Stone, J. O., 2000. Air pressure and cosmogenic isotope production. Journal of Geophysical Research 105 (B10), 23753-23759.

Stone, J. O., Allan, G. L., Fifield, L. K., Cresswell, R. G., 1996. Cosmogenic ^{36}Cl from calcium spallation. Geochimica et Cosmochimica Acta 60 (4), 679-692.

Vermeesch, P., Baur, H., Heber, V. S., Kober, F., Oberholzer, P., Schaefer, J. M., Schlüchter, C., Strasky, S., Wieler, R., 2009. Cosmogenic ^{3}He and ^{21}Ne measured in quartz targets after one year of exposure in the Swiss Alps. Earth and Planetary Science Letters 284 (3-4), 417-425.

Table captions:

Table 1: Sample details. Geographic sample locations, scaling factors for neutron induced and slow negative muon induced reactions calculated according to Stone (2000), sample thickness and thickness correction factors for spallation reactions.

Table 2: Element concentrations in minerals. a) Concentrations of target elements for ^{36}Cl production in pretreated pyroxene separates (px) and one plagioclase separate (plg) before ^{36}Cl extraction, determined by ICP-OES at the SARM (CRPG, France). "< D.L." = "below detection limit". b) Concentrations of U, Th and Li in chemically untreated pyroxene (px) and olivine (ol) separates, determined by ICP-MS (U, Th) and atomic absorption (Li) at SARM. c) Concentrations of target elements for ^{21}Ne production in chemically untreated pyroxene and olivine separates determined by electron microprobe at the Université Henri Poincaré on 6-8 grains (mean values and their standard deviations). Calculated elemental production rates for ^{21}Ne according to Masarik (2002) are also shown.

Table 3: Cosmogenic components of the measured ^{36}Cl, ^{3}He and ^{21}Ne concentrations and their ratios, with mean values and standard deviations, in a) pyroxene and b) olivine separates. Note that the ^{36}Cl concentrations of samples TZ10 and TZ12 are mean values of the two replicates of each (Table A1) with the corresponding standard deviations.

Table 4: Apparent exposure ages calculated using the cosmogenic ^{36}Cl, ^{3}He and ^{21}Ne concentrations in pyroxene (Table 3) and the SLHL production rates detailed in the footnotes. ^{36}Cl exposure ages were calculated with the ^{36}Cl calculation spreadsheet (Schimmelpfennig et al., 2009). Note that the ^{36}Cl exposure ages for samples TZ10 and TZ12 are mean values of the exposure ages of the two replicates of each with the corresponding standard deviations. The uncertainties (1σ) of the exposure ages do not include the uncertainties in the SLHL production rates, but those in the cosmogenic nuclide concentrations and for ^{36}Cl those in the contributions of the production reactions other than spallation.

Figure captions

Fig. 1: Sample location. a) Google Maps satellite image of Mt. Kilimanjaro, Tanzania. b) Side face (NW-SE) of Mt. Kilimanjaro (Image PIA03355, Courtesy NASA/JPL-Caltech), showing its peaks Shira, Kibo and Mawenzi as well as the sample locations and altitudes. Topography is vertically exaggerated two times.

Fig. 2: Cosmogenic ^{3}He concentrations in olivine and pyroxene phenocrysts. The red lines represent the mean values of the concentrations in pyroxene. For sample TZ09 ^{3}He was only measured in pyroxene.

Fig. 3: Neon three-isotope diagram showing data from olivines and pyroxenes at two temperature steps. The regression line defines a spallation line, which passes through the air component and is indistinguishable from the air-spallation mixing line of Schäfer et al. (1999).

Fig. 4: TCN ratios, calculated from the total cosmogenic ^{3}He, ^{21}Ne and ^{36}Cl concentrations, as a function of altitude. Black circles correspond to the ratios in pyroxene, gray circles to those in olivine. The continuous and dashed lines indicate the means of the ratios and their standard deviations, respectively, with values given to the left.

Fig. 5: Exposure age ratios calculated from cosmogenic ^{36}Cl, ^{3}He and ^{21}Ne concentrations in pyroxene. Production rates used are: 48.8 atoms (g Ca)$^{-1}$ a^{-1} for ^{36}Cl (Stone et al., 1996), 128 atoms (g mineral)$^{-1}$ a^{-1} for ^{3}He (Blard et al., 2006) and 25 atoms (g mineral)$^{-1}$ a^{-1} for ^{21}Ne (Fenton et al., 2009). Standard deviations of these production rates are not propagated in the ratio uncertainties (see Table 4). The black circles at the altitude of sample TZ15 in panels a) and b) represent the age ratios when assuming the highest possible correction for radiogenic ^{4}He*, while the open circles mark the ratios if no such correction is done (see text for details). The black circle at the altitude of TZ09 in panel a) represents the age ratio ignoring erosion, while the open diamond represents the ratio if erosion is taken into account (see text for details).

Fig. 6: ^{36}Cl/^{3}He exposure age ratios as in Fig. 5a with apparent altitudinal trend. TZ15 is not considered due to uncertain cosmogenic ^{3}He concentrations, and the TZ09 composition has been corrected for erosion (section 4.2). The 40% increase of the ^{3}He/^{10}Be trend in Himalayan zircons between 3200 and 4800 m

(Amidon et al., 2008) is indicated in gray. Note that here $^{10}Be/^{3}He$ concentration ratios are compared to $^{36}Cl/^{3}He$ exposure age ratios.

Table 1

Sample	Latitude South	Longitude East	Altitude [m]	Scaling neutrons	Scaling muons	Thickness [cm]	Thickness correction
TZ09	03°23.740’	37°30.248’	1013	1.27	0.95	5.3	0.957
TZ10	03°10.490’	37°31.180’	2740	3.94	1.95	5.8	0.953
TZ12	03°10.490’	37°31.180’	2740	3.94	1.95	5.7	0.953
TZ13	03°09.319’	37°30.411’	3050	4.69	2.19	4.5	0.963
TZ14	03°09.319’	37°30.411’	3050	4.69	2.19	5.1	0.958
TZ17	03°08.308’	37°28.791’	3694	6.56	2.75	6.8	0.945
TZ15	03°07.020’	37°28.234’	4107	8.02	3.16	4.2	0.965
TZ19	03°05.791’	37°25.240’	4331	8.90	3.39	7.2	0.942

Table 2

a)

Sample	Ca [%]	K [%]	Ti [%]	Fe [%]
TZ09 (px)	13.87±0.28	< D.L.	0.88±0.04	5.71±0.11
TZ10A (px)	15.71±0.31	< D.L.	1.37±0.07	4.66±0.09
TZ10B (px)	15.69±0.31	< D.L.	1.38±0.07	4.68±0.09
TZ12A (px)	15.56±0.31	< D.L.	1.37±0.07	4.65±0.09
TZ12B (px)	15.48±0.31	< D.L.	1.33±0.07	4.77±0.10
TZ13 (px)	15.19±0.30	< D.L.	1.16±0.06	4.64±0.09
TZ14 (px)	15.14±0.30	< D.L.	1.11±0.05	4.58±0.09
TZ17 (px)	15.22±0.31	0.04±0.01	1.16±0.06	4.57±0.09
TZ15 (px)	13.06±0.26	< D.L.	0.98±0.05	7.61±0.15
TZ19 (px)	15.44±0.31	< D.L.	1.49±0.07	5.32±0.10
TZ15 (plg)	7.46±0.15	0.50±0.02	0.10±0.01	0.45±0.01

b)

Sample	U [ppm]	Th [ppm]	Li [ppm]
TZ09 (px)	0.039	0.156	3.2
TZ12 (px)	0.079	0.443	2.9
TZ14 (px)	0.113	0.455	2.3
TZ17 (px)	0.100	0.460	< D.L.
TZ15 (px)	0.086	0.282	4.5
TZ19 (px)	0.123	0.546	7.0
TZ12 (ol)	0.042	0.059	< D.L.
TZ14 (ol)	0.038	0.062	2.4
TZ17 (ol)	0.068	0.030	2.0
TZ15 (ol)	0.086	0.165	6.8
TZ19 (ol)	0.035	0.038	2.4

c)

Sample	Mg [%]	Al [%]	Si [%]	Ca [%]	Fe [%]	Na [%]
TZ10/12 (px)	8.06±0.43	3.70±0.30	22.24±0.52	16.23±0.22	4.60±0.40	0.55±0.04
TZ13/14 (px)	8.85±0.58	3.03±0.50	23.23±0.62	15.73±0.34	4.20±0.48	0.56±0.02
TZ17 (px)	10.04±0.24	1.97±0.26	24.32±0.25	15.34±0.21	3.33±0.13	0.51±0.03
TZ15 (px)	9.17±0.68	1.65±0.24	23.92±0.46	14.45±0.54	7.03±1.47	0.35±0.03
TZ10/12 (ol)	26.13±0.64	0.01±0.03	18.76±0.24	0.39±0.30	12.96±1.03	0.02±0.03
TZ13/14 (ol)	25.79±0.73	0.01±0.03	18.64±0.17	0.26±0.14	13.46±1.06	0.02±0.02
Elemental Prod. rates [a]	175.1	62.4	41.7	1.8	0.2	102.0

[a] [atoms ^{21}Ne (g element)$^{-1}$ a^{-1}]

Table 3

a) Pyroxene

Sample	$^{36}Cl_{cos}$ (px) [10^6 atoms g^{-1}]	$^{3}He_{cos}$ (px) [10^6 atoms g^{-1}]	$^{21}Ne_{cos}$ (px) [10^6 atoms g^{-1}]	[^{36}Cl]/[^{3}He] (px)	[^{21}Ne]/[^{3}He] (px)	[^{36}Cl]/[^{21}Ne] (px)
TZ09	0.631±0.017	9.60±0.29		0.0658±0.0027		
TZ10	4.246±0.065	73.8±1.1	13.52±0.44	0.0576±0.0012	0.1834±0.0066	0.314±0.011
TZ12	4.029±0.074	66.2±2.1	12.91±0.60	0.0608±0.0022	0.195±0.0011	0.312±0.016
TZ13	4.94±0.12	93.5±2.7	16.62±0.67	0.0529±0.0020	0.1780±0.0089	0.297±0.014
TZ14	5.25±0.10	99.8±2.3	18.96±0.69	0.0526±0.0016	0.1899±0.0082	0.277±0.011
TZ17	2.059±0.059	32.1±2.2[a]	6.30±0.53	0.0642±0.0048	0.196±0.021	0.327±0.029
TZ15	0.781±0.021	15.84±0.78	2.79±0.14	0.0493±0.0028	0.176±0.012	0.279±0.016
TZ19	1.47±0.10	23.5±1.1[a]		0.0626±0.0052		
Mean ± st. dev.				0.0582±0.0061	0.1864±0.0085	0.301±0.020

b) Olivine

Sample	$^{3}He_{cos}$ (ol) [10^6 atoms g^{-1}]	$^{21}Ne_{cos}$ (ol) [10^6 atoms g^{-1}]	[^{21}Ne]/[^{3}He] (ol)
TZ10	67.7±1.8	26.8±1.4	0.396±0.023
TZ12	66.9±1.4	24.8±1.2	0.371±0.019
TZ13	85.7±1.4	32.8±1.4	0.383±0.017
TZ14	97.9±7.7	34.9±2.2	0.357±0.061
TZ17	34.88±0.54		
TZ15	13.13±0.59		
TZ19	22.84±0.52		
Mean ± st. dev.			0.377±0.018

[a] Magmatic $^{3}He/^{4}He$ values were determined applying the isochron method by Blard and Pik (2008)

Table 4

Sample	^{36}Cl (px) [a] [ka]	^{3}He (px) [b] [ka]	^{21}Ne (px) [c] [ka]
TZ09	71.7±5.4	61.7±1.9	144.3±4.7
TZ10	156.1±9.1	154±2.3	137.6±6.4
TZ12	148.7±8.7	137.9±4.4	147.5±5.9
TZ13	157±13	161.9±4.7	168.9±6.1
TZ14	171±14	173.7±4.0	40.6±3.4
TZ17	40.9±3.0	40.4±2.8	14.43±0.72
TZ15	14.4±1.0	15.98±0.78	
TZ19	21.1±2.0	21.90±1.0	

[a] ^{36}Cl SLHL production for spallation of Ca 48.8±1.7 atoms ^{36}Cl (g Ca)$^{-1}$ a^{-1} according to Stone et al. (1996)
[b] ^{3}He SLHL production for pyroxene 128±5 atoms ^{3}He (g px)$^{-1}$ a^{-1} according to Blard et al. (2006)
[c] ^{21}Ne SLHL production for pyroxene 25±8 atoms ^{21}Ne (g px)$^{-1}$ a^{-1} according to Fenton et al. (2009)

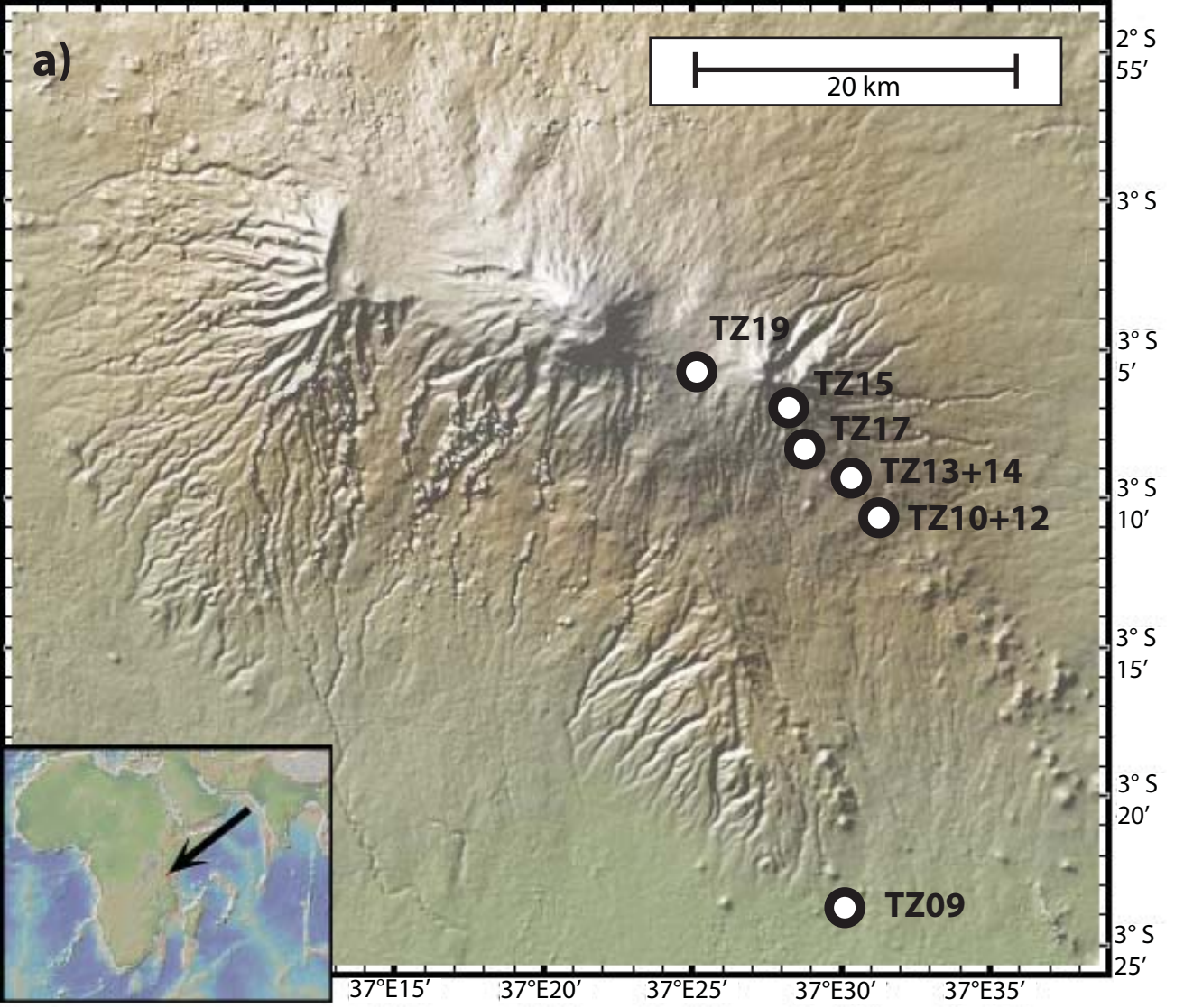
a)
20 km
TZ19
TZ15
TZ17
TZ13+14
TZ10+12
TZ09
2° S
55′
3° S
3° S
5′
3° S
10′
3° S
15′
3° S
20′
3° S
25′
37°E15′
37°E20′
37°E25′
37°E30′
37°E35′

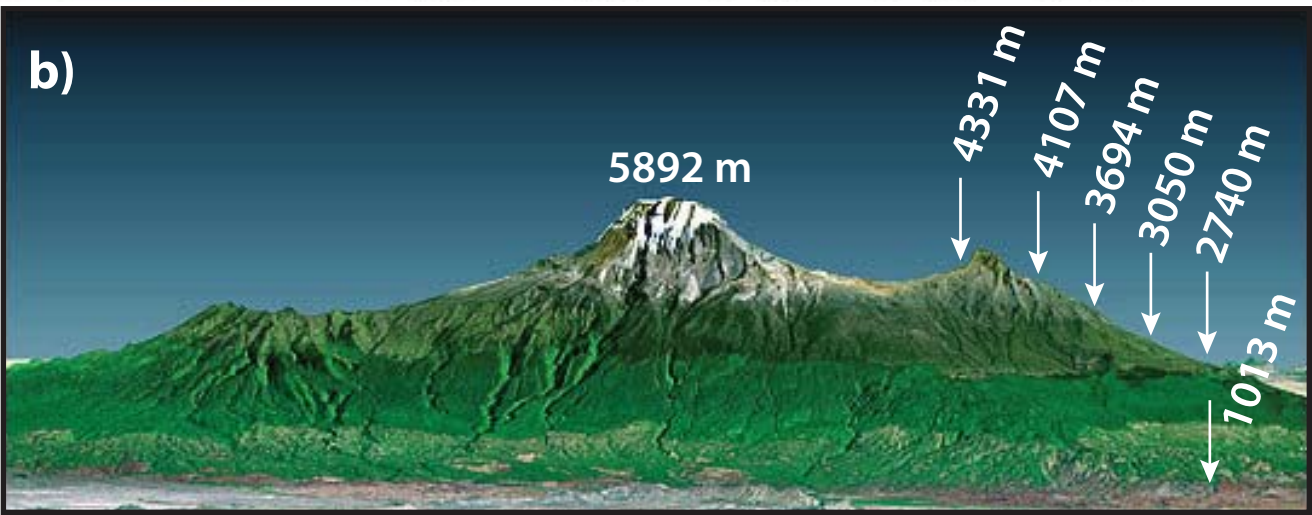
b)
5892 m
4331 m
4107 m
3694 m
3050 m
2740 m
1013 m

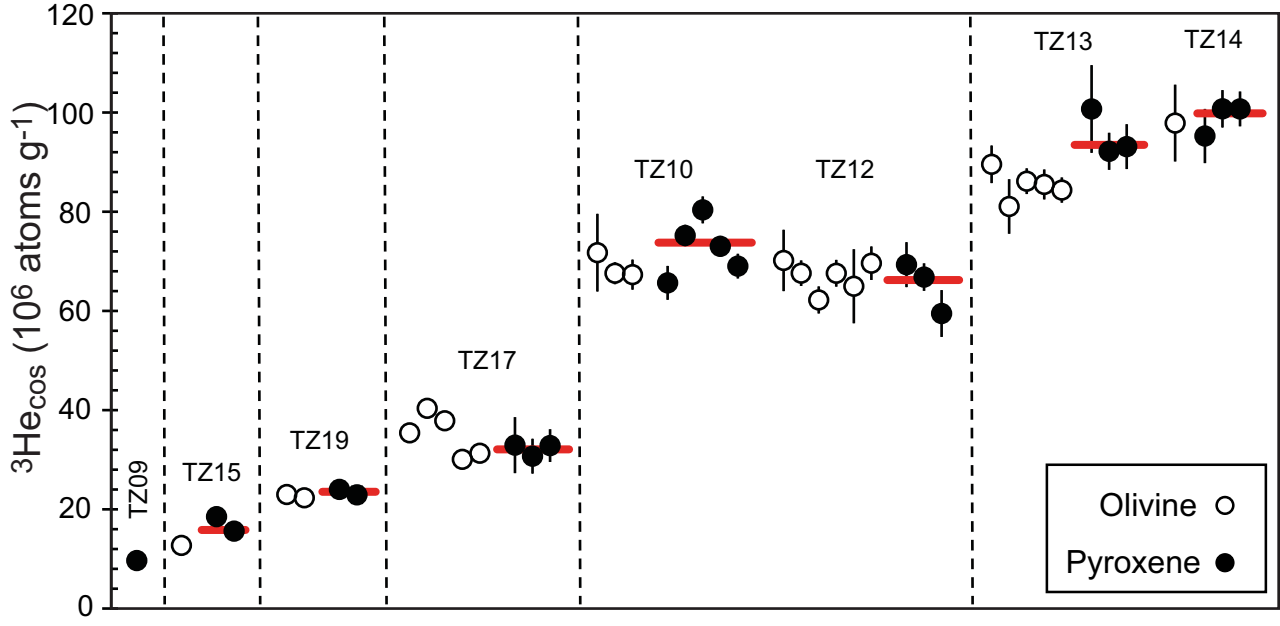
120
100
80
60
40
20
0
$^3He_{cos}$ (10^6 atoms g^{-1})
TZ09
TZ15
TZ19
TZ17
TZ10
TZ12
TZ13
TZ14
Olivine
Pyroxene

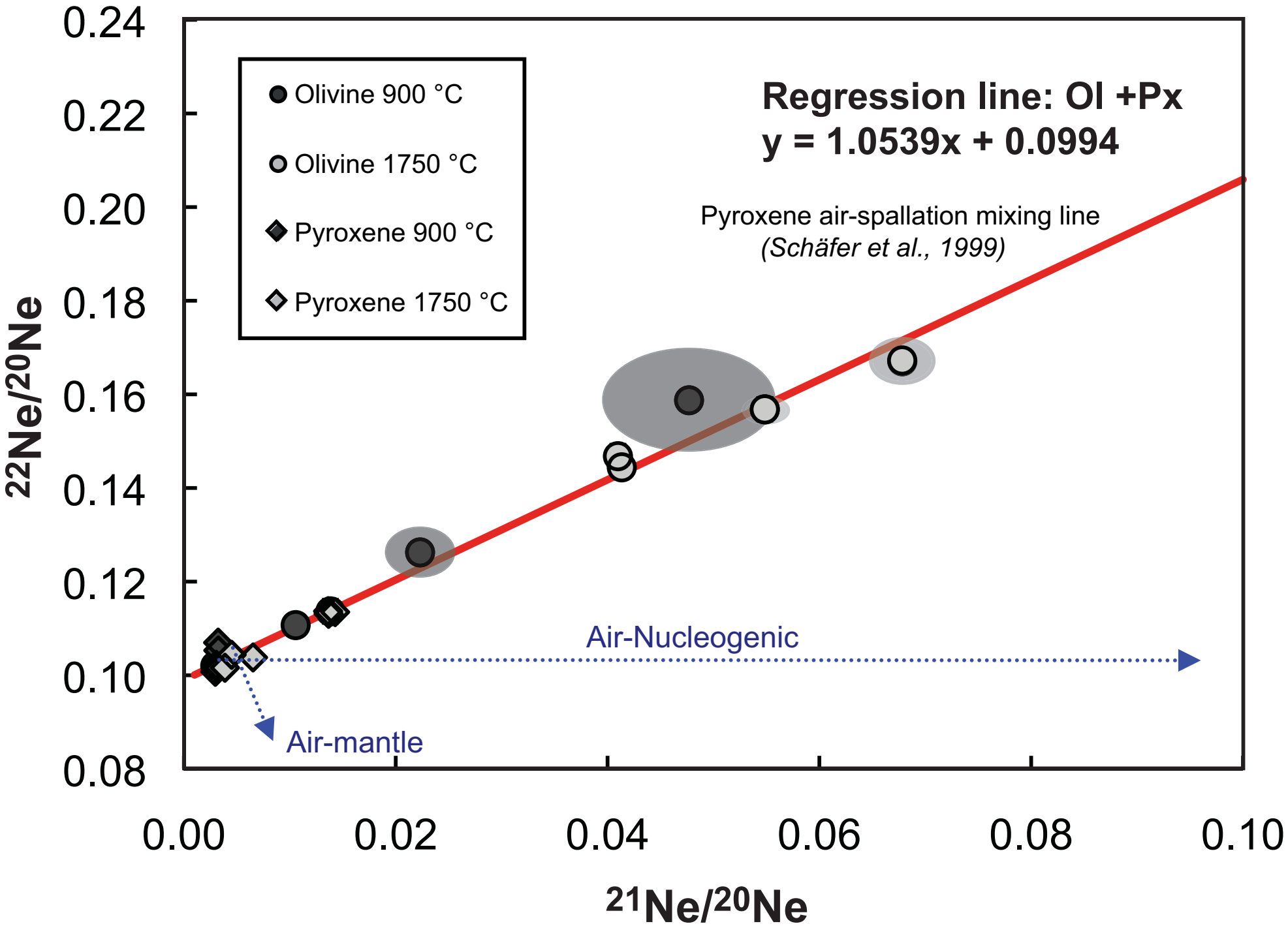
Olivine 900 °C
Olivine 1750 °C
Pyroxene 900 °C
Pyroxene 1750 °C
Regression line: Ol +Px
y = 1.0539x + 0.0994
Pyroxene air-spallation mixing line
(Schäfer et al., 1999)
Air-Nucleogenic
Air-mantle
0.24
0.22
0.20
0.18
0.16
0.14
0.12
0.10
0.08
0.00
0.02
0.04
0.06
0.08
0.10
22Ne/20Ne
21Ne/20Ne

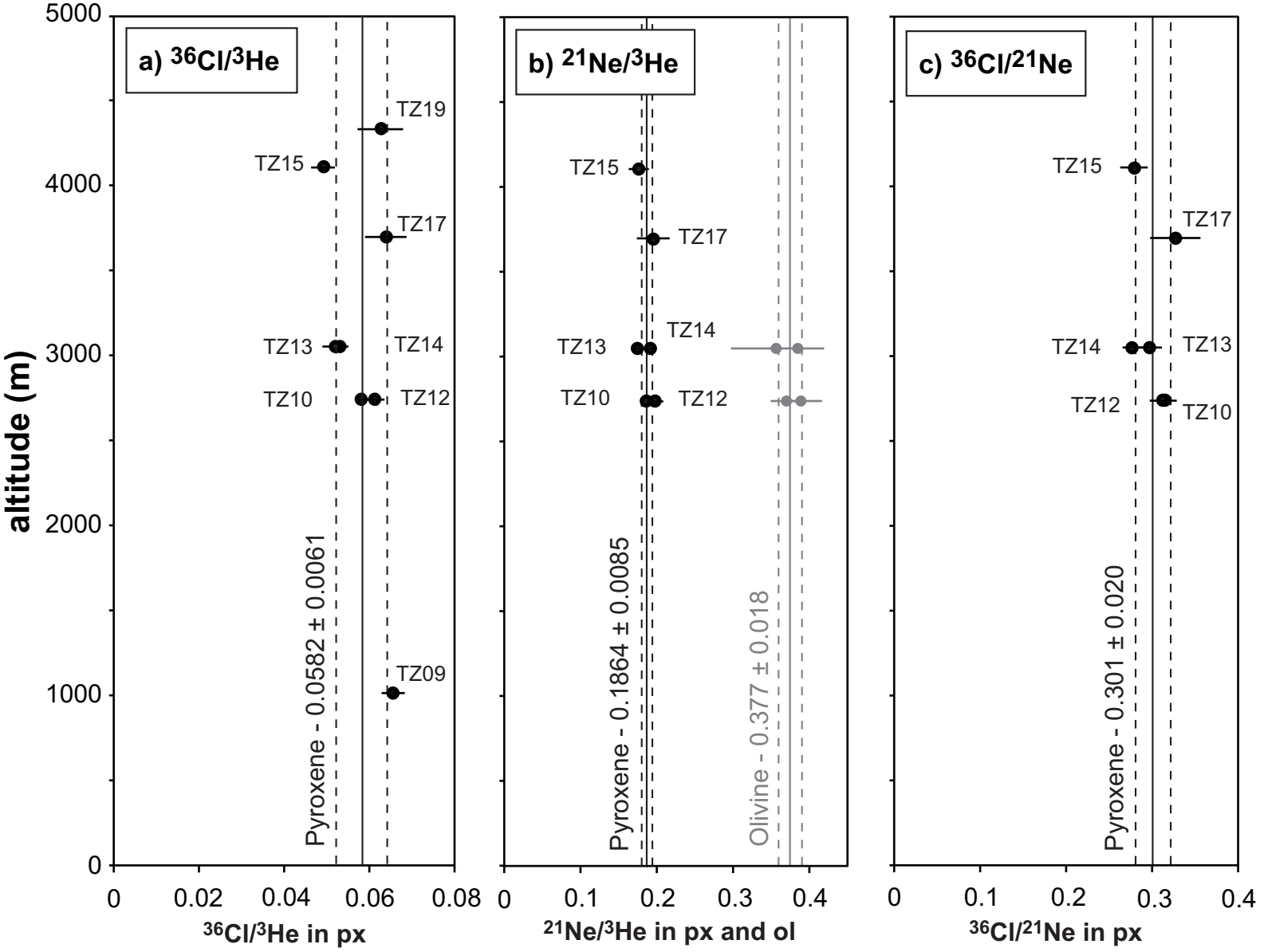
a) 36Cl/3He
b) 21Ne/3He
c) 36Cl/21Ne
altitude (m)
5000
4000
3000
2000
1000
0
TZ19
TZ15
TZ17
TZ13
TZ14
TZ10
TZ12
TZ09
Pyroxene - 0.0582 ± 0.0061
Pyroxene - 0.1864 ± 0.0085
Olivine - 0.377 ± 0.018
Pyroxene - 0.301 ± 0.020
0
0.02
0.04
0.06
0.08
0.1
0.2
0.3
0.4
36Cl/3He in px
21Ne/3He in px and ol
36Cl/21Ne in px

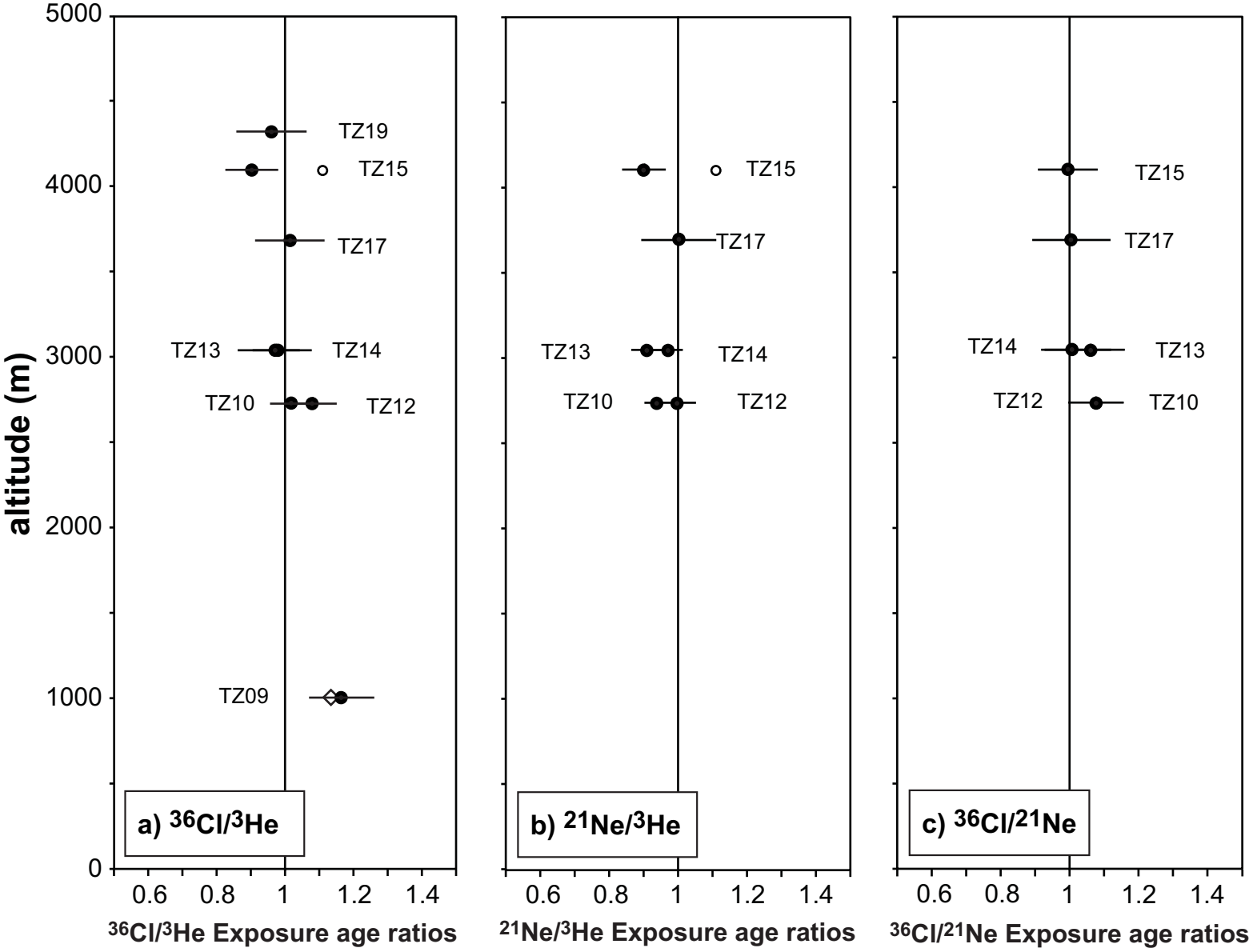
altitude (m)
5000
4000
3000
2000
1000
0
TZ19
TZ15
TZ17
TZ13
TZ14
TZ10
TZ12
TZ09
a) 36Cl/3He
0.6
0.8
1
1.2
1.4
36Cl/3He Exposure age ratios
TZ15
TZ17
TZ13
TZ14
TZ10
TZ12
b) 21Ne/3He
21Ne/3He Exposure age ratios
TZ15
TZ17
TZ14
TZ13
TZ12
TZ10
c) 36Cl/21Ne
36Cl/21Ne Exposure age ratios

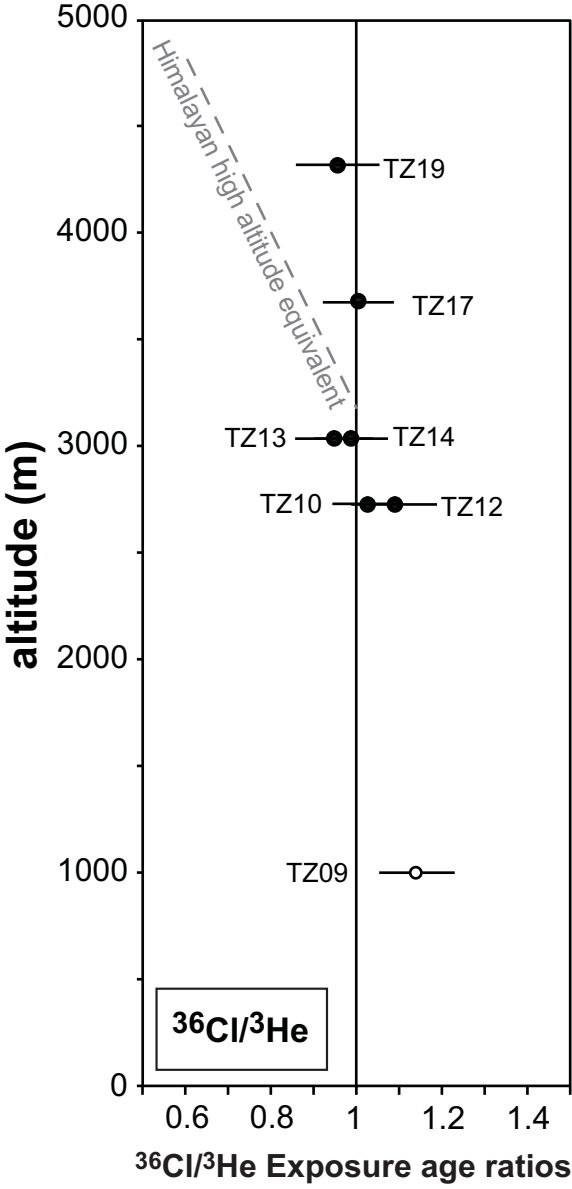
5000
4000
3000
2000
1000
0
altitude (m)
Himalayan high altitude equivalent
TZ19
TZ17
TZ13
TZ14
TZ10
TZ12
TZ09
36Cl/3He
0.6
0.8
1
1.2
1.4
36Cl/3He Exposure age ratios

Appendix for the manuscript:

Inter-comparison of cosmogenic in-situ ^{3}He, ^{21}Ne and ^{36}Cl at low latitude along an altitude transect on the SE slope of Kilimanjaro volcano (3°S, Tanzania)

by Irene Schimmelpfennig*, Alice Williams, Raphaël Pik, Pete Burnard, Samuel Niedermann, Robert Finkel, Björn Schneider, Lucilla Benedetti

* corresponding author: schimmel@ldeo.columbia.edu, irene.lois@yahoo.de

Quaternary Geochronology

Sample site descriptions

- Sample TZ09 (1013 m): Ropey but eroded tumuli surface of a pyroxene-rich (~3 mm) "red" basalt flow on Mui Crater in the Kilemo Zone on the southern slopes of Kilimanjaro (Fig. A1a).
- Sample TZ10 (2740 m): 30 cm-high well-preserved hornito on the surface of an ankaramitic lava flow at the edge of the rainforest in the Rombo Zone (Fig. A1b).
- Sample TZ12 (2740 m): Flat tumulus surface taken a few meters from TZ10 on the same flow.
- Sample TZ13 (3050 m): Set of three preserved pahoehoe ropes of an ankaramitic lava flow in the Rombo Zone (Fig. A1c).
- Sample TZ14 (3050 m): Flat edge of small, 1 m-wide tumulus a few meters from TZ13 on the same ankaramitic flow (Fig. A1d).
- Sample TZ15 (4107 m): Surface of a 3 m-wide, glacially polished doleritic dyke (Fig. A1e). Contains large plagioclase laths and pyroxene phenocrysts and minor olivine (<2 mm).
- Sample TZ17 (3694 m): Vesicular but fresh sample taken from the degraded ropey surface of a rubbly ankaramitic lava flow near the top of a small parasitic cone in the Rombo Zone (Fig. A1f).
- Sample TZ19 (4331 m): Surface of an eroded ankaramitic pressure-ridge, small upper areas of which exhibit minor polishing. Low vesicularity. Contains abundant fresh olivine and pyroxene phenocrysts (Fig. A1g).

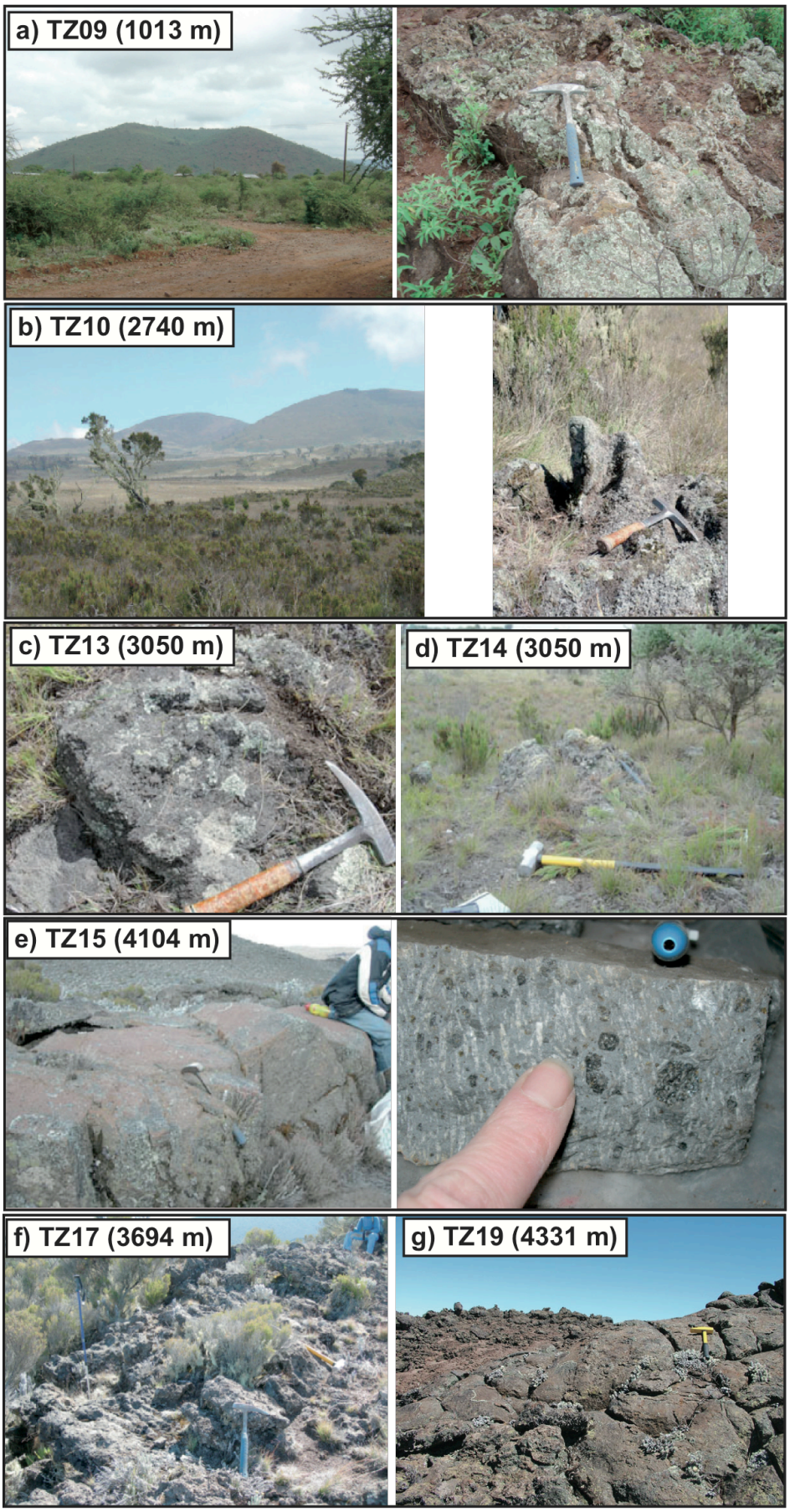

Fig. A1: Pictures of sample sites at Kilimanjaro.

Chemical ^{36}Cl extraction

Chemical ^{36}Cl extractions were conducted at CEREGE. Initial mineral weights ranged between 3.5 g and 10.5 g. Grains were first washed with MQ water in closed HDPE bottles for several hours on a shaker table, then etched in limited amounts of a HF (40%)/ HNO_3 (10%) mixture (volume ratio 1:2) in order to dissolve about 20% of the grains and ensure total groundmass removal. From the etched grains an aliquot of 1 g was taken for chemical composition analysis at SARM (CRPG, Nancy, France). The remainder was dissolved with an excess amount of the HF/HNO_3 mixture by shaking overnight. Prior to dissolution, approximately 1.5 mg of chloride in the form of a chloride carrier (OakRidge National Laboratory), enriched in ^{35}Cl (99.9%), was added to the solution. After complete dissolution of the grains, the solutions were centrifuged to separate the supernatant from the fluoric cake formed during the dissolution reaction. AgCl was precipitated by adding $AgNO_3$. This first precipitate was re-dissolved in dilute NH_4OH, and, in order to reduce the isobaric interferences of ^{36}S during the ^{36}Cl AMS measurements, $Ba(NO_3)_2$ was added to precipitate $BaSO_4$/$BaCO_3$. The AgCl was again precipitated from the resulting solution by acidification with HNO_3 and collected by centrifuging. Finally, the AgCl precipitates were rinsed and dried in preparation for measurement at LLNL-CAMS. AgCl yields, including carrier and natural Cl, accounted for 4 to 6 g.

Table A1: ^{36}Cl data from AMS measurements at LLNL-CAMS with sample weight, amount of spike-Cl and calculated Cl and ^{36}Cl concentrations in pyroxene separates and in one plagioclase separate (TZ15-plg). Note that replicates were measured for samples TZ10 and TZ12. Uncertainties correspond to 1σ.

Sample	sample weight dissolved [g]	measured ^{35}Cl/ ^{37}Cl	measured ^{36}Cl/ ^{35}Cl [10^{-14}]	Cl content in spike [mg]	[Cl] in sample [ppm]	[^{36}Cl] [10^6 atoms g^{-1}]
TZ09	4.52	230.2± 2.0	11.99± 0.28	1.457	2.68± 0.25	0.631± 0.017
TZ10A	2.63	247.8± 1.6	44.03± 0.74	1.475	4.60± 0.38	4.201± 0.083
TZ10B	1.84	341.9± 2.4	32.05± 0.62	1.473	2.77± 0.38	4.31± 0.11
TZ12A	2.80	238.3± 2.9	46.0± 1.1	1.484	4.43± 0.40	4.16± 0.11
TZ12B	2.79	253.64± 0.15	43.1± 1.0	1.484	3.86± 0.35	3.90± 1.0
TZ13	4.17	177.17± 0.10	80.2± 1.9	1.488	5.21± 0.36	4.94± 0.12
TZ14	3.75	188.13± 0.59	77.3± 1.4	1.478	5.18± 0.37	5.25± 0.10
TZ17	2.01	178.3± 2.5	16.88± 0.40	1.467	10.06± 0.79	2.059± 0.059
TZ15	3.41	239.5± 4.4	11.27± 0.27	1.459	3.18± 0.34	0.781± 0.021
TZ19	6.42	91.0± 7.0	37.5± 2.6	1.451	8.41± 0.98	1.47± 0.10
TZ15-plg	7.52	300.0± 5.9	16.08± 0.31	1.457	0.74± 0.12	0.514± 0.011
Blanks						
BL-1		418.6± 6.8	0.72± 0.10	1.461		
BL-2		412.1± 1.9	0.77± 0.05	1.460		
BL-3		447.8± 1.2	0.85± 0.10	1.483		
BL-4		474.78± 0.10	0.90± 0.06	1.473		

Table A2: Bulk rock composition determined at SARM (CRPG, Nancy, France).

sample	SiO_2 [%]	Al_2O_3 [%]	Fe_2O_3 [%]	CaO [%]	MgO [%]	Na_2O [%]	K_2O [%]	TiO_2 [%]	MnO [%]
TZ09	44.62	11.51	14.51	10.69	8.64	2.12	0.95	3.07	0.21
TZ10	39.16	11.84	13.54	13.50	11.22	2.28	0.76	3.85	0.19
TZ12	39.16	11.84	13.54	13.50	11.22	2.28	0.76	3.85	0.19
TZ13	39.64	11.44	13.98	12.60	12.80	1.79	0.85	3.52	0.19
TZ14	39.64	11.44	13.98	12.60	12.80	1.79	0.85	3.52	0.19
TZ17	40.00	11.67	13.34	12.94	10.71	1.71	1.13	4.00	0.17
TZ15	48.52	14.88	13.08	7.80	6.03	3.56	1.71	3.01	0.16
TZ19	39.25	11.69	14.68	12.97	10.06	2.98	1.19	3.89	0.21

	P_2O_5 [%]	H_20 [%]	Cl [ppm]	Li [ppm]	B [ppm]	Sm [ppm]	Gd [ppm]	Th [ppm]	U [ppm]
TZ09	0.69	2.01	105	5.8	4.5	8.9	8.0	4.7	0.7
TZ10	0.70	4.02	150	6.6	3.4	12.9	9.7	10.7	2.3
TZ12	0.70	4.02	150	6.6	3.4	12.9	9.7	10.7	2.3
TZ13	0.56	3.25	570	7.5	4.1	11.3	8.6	7.9	1.7
TZ14	0.56	3.25	570	7.5	4.1	11.3	8.6	7.9	1.7
TZ17	0.62	2.90	435	4.3	3.9	12.2	9.6	9.3	2.1
TZ15	0.52	0.33	81	11.1	2.8	9.0	7.7	6.0	0.9
TZ19	0.80	2.23	195	7.4	4.8	14.4	10.4	11.2	2.5

Helium and neon measurements and standards

At CRPG, He isotope concentrations and ratios were measured on GV Instruments Helix Split Flight Tube and Helix Multi-collector mass-spectrometers. Cross-calibrations of the mass-spectrometers and their purification lines were made using the HESJ Helium gas standard (Matsuda et al., 2002), which has a certified $^3He/^4He$ of 20.63 ± 0.10 R_A. Daily measurements of standard-aliquots, at pressures equivalent to those of typical samples, were performed throughout the analytical periods in order to monitor the stability and sensitivity of the mass spectrometers. Further details of analytical techniques and data-reduction procedures at CRPG can be found in Zimmermann et al. (submitted).

At GFZ, He and Ne concentrations and isotopic ratios were determined in a VG5400 mass spectrometer. After gas extraction (see next section), chemically active gases were removed in two Ti sponge and two SAES (ZrAl) getters, and He, Ne, and Ar-Kr-Xe were separated from each other by trapping in a cryogenic adsorber and subsequent sequential release. Corrections for isobaric interferences of $^{40}Ar^{++}$ and CO_2^{++} were applied according to the method described in Niedermann et al. (1993, 1997), which takes account of variations in charge state ratios depending on the mass spectrometer background. Typically, the corrections amounted to <10% of the ^{20}Ne and <5% of the ^{22}Ne signal, but contributed up to 20% of ^{20}Ne and 50% of ^{22}Ne in a few extreme cases. Owing to the small uncertainties of the correction factors (<10% at the 2σ level) even such high corrections do not significantly affect the precision of the results. Analytical blanks were (1 to 8) × 10^8 atoms ^4He and (2 to 5) × 10^7 atoms ^{20}Ne, depending on extraction temperature, with atmospheric isotopic compositions. More details about the analytical methods and data reduction procedures can be found in Niedermann et al. (1997).

Measurements of the CRONUS-Earth pyroxene He standard, "P", were undertaken at both CRPG and GFZ. The measured $^{3}He_{cos}$ concentrations were 4.95 ± 0.10 × 10^{9} at g^{-1} at CRPG (mean of 6 analyses), and 4.97 ± 0.21 × 10^{9} at g^{-1} at GFZ (mean of three analyses). Aliquots of the 0.25 - 0.5 mm CRONUS-EU CREU-1 quartz neon standard were analyzed at GFZ and an excess cosmogenic ^{21}Ne concentration (relative to atmospheric composition) of 3.28 ± 0.08 × 10^{8} at g^{-1} was determined.

Noble gas extractions

Crushing experiments

In vacuo crushing of olivines and pyroxenes was performed at CRPG for determination of magmatic $^{3}He/^{4}He$ in samples TZ10, TZ12, TZ13 and TZ14. Crush experiments were conducted using steel tubes containing iron slugs activated by external solenoids. Approximately 1 g of each phenocryst sample was loaded into the crushers, and baked under vacuum at 110°C overnight. After cooling to room temperature, samples were crushed during a 2-minute period (at a rate of 100 strokes/min). Total He released ranged from 0.03 to 11.70 × 10^{11} atoms g^{-1} and was consistently lower in olivine samples (mean pyroxene = 7.16 × 10^{11} atoms g^{-1}; mean olivine = 0.12 × 10^{11} atoms g^{-1}). Because of the low He-yield from olivines, possibly indicative of a scarcity of melt/fluid inclusions, the measured $^{3}He/^{4}He$ values were associated with large uncertainties (up to 70%). In contrast, calculated $^{3}He/^{4}He$ in pyroxenes ranged from 6.2 to 6.6 R_A, with individual measurement uncertainties of 2 to 7%. Note that this value is consistent with a previous determination of the mantle $^{3}He/^{4}He$ signature at Mt. Kilimanjaro (6.7 ± 0.1 R_A, Pik et al., 2006).

Melt extractions

High-temperature melting experiments were performed in the noble gas laboratories at both CRPG (He only) and GFZ (He and Ne). At CRPG, 0.11 - 0.25 g aliquots of pure olivine or pyroxene phenocrysts were wrapped in Cu-foil, loaded into the sample carousel (n = 20) and baked under vacuum at 110°C over a 3-day period. After total degassing of the extraction furnace over several hours, the furnace temperature was maintained at 800°C prior to sample introduction. Each sample was dropped into the Ta-crucible and heated to 1450°C over a 20-minute period, before reduction of the furnace temperature to 800°C and introduction of the gas to the purification line. Repeat extractions ensured total extraction of He.

At GFZ, aliquots of 0.25 - 1.50 g pure olivine and pyroxene were wrapped in Al-foil and placed in the sample carousel, where they were baked under vacuum for about one week at 100°C. Noble gases were extracted in two heating steps of 900°C and 1750°C, enabling partial separation of atmospheric and radiogenic from cosmogenic components.

Magmatic $^{3}He/^{4}He$ determinations for calculation of cosmogenic ^{3}He

Magmatic $^{3}He/^{4}He$ values were determined either from the crushing experiments described above (samples TZ10, TZ12, TZ13 and TZ14) or, when there was insufficient material for crushing experiments, using isochron intercept values (TZ17, TZ19). In vacuo crushing of phenocrysts releases magmatic He contained within fluid and melt inclusions in the crystals. Magmatic $^{3}He/^{4}He$ normally vary little within phenocryst populations of individual lava flows and crushing of single olivine and pyroxene aliquots is generally considered adequate for determining the magmatic He composition of a flow. Because of the large uncertainties

associated with the crush-data for Kilimanjaro olivines (see previous section), we used the co-genetic pyroxene $^{3}He/^{4}He$ values for calculations of olivine cosmogenic ^{3}He. Magmatic $^{3}He/^{4}He$ signatures of pyroxenes usually deviate little from those of co-existing olivines. Furthermore, in this study small variations in the magmatic ratio will have a negligible effect on calculated cosmogenic ^{3}He since the melt extractions of He from olivines of these four samples also yielded low ^{4}He concentrations (Table A3).

For samples TZ17 and TZ19, crushing experiments were not successfully determined and we inferred their magmatic $^{3}He/^{4}He$ values from the isochron method recently proposed by Blard and Pik (2008) (Fig. A2 b and c). In the $(^{3}He/^{4}He)_{tot}$ vs $1/^{4}He_{tot}$ space, a suite of data define a straight line, its intercept representing the magmatic $(^{3}He/^{4}He)_{mag}$ ratio, and its slope the cosmogenic ^{3}He concentration. Using optimized total extraction apparatus it allows precise determination of cosmogenic ^{3}He by increasing the number of measured aliquots. The method has the additional advantage of avoiding a preliminary crushing step and potential loss of cosmogenic helium (Blard et al., 2006). Cosmogenic ^{3}He concentrations should be identical whichever method is used to calculate them (compare Fig. A2 and values in Table A3), however, the isochron method allows a better assessment of data-set consistency via its graphical output, and also necessitates an increase in the number of replicates which in turn improves the statistical determination of the cosmogenic concentrations. For TZ17 and TZ19, the magmatic $^{3}He/^{4}He$ values determined by the isochron method were 6.1 ± 0.4 and 6.3 ± 0.4 R_A, respectively.

For samples TZ09 and TZ15, an insufficient number of aliquots were analyzed to construct cosmogenic isochrons. For these samples we therefore used the mean $^{3}He/^{4}He$ of the magmatic $^{3}He/^{4}He$ values presented above (6.4 ± 0.2 R_A). Given the very homogeneous ratios determined for the other samples in this study we consider this approximation to be sufficiently reliable.

$^{40}Ar/^{39}Ar$ age determination: sample TZ15

$^{40}Ar/^{39}Ar$ dating was conducted on sample TZ15 at the noble gas laboratory at Vrije Universiteit, Amsterdam (Netherlands), following the methods described in Koppers et al. (2000) and Schneider et al. (2009). Groundmass was prepared by hand-picking 250-500 μm size grains under a binocular microscope to remove those containing alteration, vesicles or phenocrysts. After cleaning in dilute HNO_3, approximately 1 g of grains was wrapped in Al-foil and sent for 1-hour irradiation at the RODEO facility in the ECN HFR nuclear reactor, Petten, Netherlands. Several aliquots of the internal DRA-1 sanidine standard were also included. Following a cool-down period to allow ^{37}Ar activity to return to safe levels, the sample was loaded in an all-metal sample carousel at the AGES facility in the noble gas laboratory in the Faculty of Earth and Life Science at the Vrije Universiteit Amsterdam, and baked overnight at 500 °C. Ten $^{40}Ar/^{39}Ar$ incremental heating steps were conducted between 650 and 1250 °C (Table A5). The resulting plateau $^{40}Ar/^{39}Ar$ age of 527.3 ± 4.9 ka is concordant with the isochron (normal and reverse) and total fusion ages (Fig. A3).

Table A3: Helium data for pyroxene and olivine separates. Measurements were performed at CRPG Nancy on the GV Instruments Helix SFT and Helix MC mass spectrometers and at GFZ Potsdam on a VG 5400 mass spectrometer (labeled *). Data have been corrected for blanks and calibrated against local gas standards that agree for ^{3}He cross calibration within ~ 3%. Uncertainties correspond to 1σ. Cosmogenic ^{3}He concentrations have been corrected for radiogenic He (^{4}He*) following the "R factor" procedure of Blard and Pik (2008) for non-eroded volcanic surfaces (TZ10, TZ12, TZ13, TZ14) or the ingrowth/implantation correction of Farley et al. (2006) for the other samples. Magmatic isotopic ratios of samples TZ10, TZ12, TZ13 and TZ14 were determined by crushing. Isochron intercepts were used for samples TZ17 and TZ19, and for samples TZ09 and TZ15 the reported value is an estimate (see text for details). $^3He_{cos}$ concentrations in bold are error-weighted means.

Sample	Mineral phase	sample weight [mg]	^{4}He (melt) [10^{12} at g^{-1}]	^{3}He (melt) [10^6 at g^{-1}]	^{3}He/^{4}He (melt) R/R_A	^{3}He/^{4}He magmatic R/R_A	P ^{4}He [10^5 at $g^{-1}a^{-1}$]	R factor	$^3He_{cos}$ [10^6 at g^{-1}]
TZ09	px	240	0.4070 ± 0.0032	12.82 ± 0.72	22.7 ± 1.3	6.40[b]	3.27	-	9.68 ± 0.74
	px	250	0.23064 ± 0.00066	11.17 ± 0.32	36.0 ± 1.1	6.40[b]	3.27	-	9.58 ± 0.32
									9.60 ± 0.29
TZ10	px*	400	1.470 ± 0.037	78.3 ± 3.3	38.3 ± 1.9	6.64	7.48	0.987	65.6 ± 3.4
	px	135	0.8957 ± 0.0022	82.4 ± 2.1	66.4 ± 1.7	6.64	7.48	0.987	75.2 ± 2.2
	px	131	2.041 ± 0.018	98.1 ± 2.4	34.67 ± 0.89	6.64	7.48	0.987	80.4 ± 2.7
	px	134	1.2108 ± 0.0034	83.2 ± 2.0	49.6 ± 1.2	6.64	7.48	0.987	73.0 ± 2.1
	px	126	2.4978 ± 0.0045	91.1 ± 1.9	26.31 ± 0.54	6.64	7.48	0.987	69.0 ± 2.5
									73.8 ± 1.1
	ol	143	0.330 ± 0.020	74.4 ± 7.8	161.6 ± 9.5	6.64	3.37	0.994	71.7 ± 7.8
	ol	207	0.0414 ± 0.0020	67.6 ± 2.2	1176 ± 69	6.64	3.37	0.994	67.6 ± 2.2
	ol*	419	0.0267 ± 0.0012	67.2 ± 3.0	1810 ± 110	6.64	3.37	0.994	67.3 ± 3.0
									67.7 ± 1.8
TZ12	px*	596	1.823 ± 0.065	85.1 ± 4.4	33.6 ± 2.1	6.61	7.48	0.987	69.3 ± 4.5
	px	243	1.0543 ± 0.0079	75.6 ± 2.7	51.4 ± 3.7	6.61	7.48	0.987	66.8 ± 2.8
	px	46	0.6830 ± 0.0039	64.9 ± 4.7	68.6 ± 5.0	6.61	7.48	0.987	59.5 ± 4.7
									66.2 ± 2.1
	ol	173	0.0698 ± 0.0032	70.4 ± 6.2	724 ± 30	6.61	3.37	0.994	70.2 ± 6.2
	ol	174	0.04097 ± 0.00084	67.6 ± 2.6	1220 ± 70	6.61	3.37	0.994	67.6 ± 2.6
	ol	186	0.03819 ± 0.00079	62.2 ± 2.7	1167 ± 65	6.61	3.37	0.994	62.2 ± 2.7
	ol	250	0.03552 ± 0.00059	67.5 ± 2.7	1351 ± 64	6.61	3.37	0.994	67.6 ± 2.7
	ol	46	0.0521 ± 0.0072	65.1 ± 7.5	900 ± 160	6.61	3.37	0.994	65.0 ± 7.5
	ol*	401	0.0403 ± 0.0019	69.6 ± 3.4	1242 ± 85	6.61	3.37	0.994	69.6 ± 3.4
									66.9 ± 1.4
TZ13	px	161	1.6121 ± 0.0041	113.46 ± 8.83	50.7 ± 1.0	6.24	8.25	0.989	100.7 ± 8.8
	px	201	3.2196 ± 0.0039	118.93 ± 3.57	26.66 ± 0.45	6.24	8.25	0.989	92.1 ± 3.7
	px*	324	2.479 ± 0.062	113.46 ± 4.4	32.9 ± 1.5	6.24	8.25	0.989	93.1 ± 4.5
									93.5 ± 2.7
	ol*	451	0.0659 ± 0.0026	89.8 ± 3.8	979 ± 56	6.24	2.85	0.996	89.6 ± 3.8
	ol	117	0.0424 ± 0.0040	81.1 ± 5.5	1380 ± 160	6.24	2.85	0.996	81.1 ± 5.5
	ol	254	0.07781 ± 0.00042	86.5 ± 2.6	802 ± 16	6.24	2.85	0.996	86.1 ± 2.6
	ol	179	0.13804 ± 0.00071	86.3 ± 3.0	451.3 ± 7.7	6.24	2.85	0.996	85.5 ± 3.0
	ol	291	0.10525 ± 0.00031	84.9 ± 2.6	582 ± 10	6.24	2.85	0.996	84.4 ± 2.6
									85.7 ± 1.4
TZ14	px*	504	2.610 ± 0.092	117.5 ± 5.4	32.4 ± 1.9	6.48	8.25	0.988	95.2 ± 5.5
	px	387	2.7523 ± 0.0025	124.2 ± 3.7	32.57 ± 0.61	6.48	8.25	0.988	100.7 ± 3.8
	px	154	1.8661 ± 0.0066	116.2 ± 3.5	44.95 ± 0.60	6.48	8.25	0.988	100.7 ± 3.5
									99.8 ± 2.3
	ol*	451	0.0879 ± 0.0051	98.2 ± 7.7	804 ± 79	6.48	2.85	0.996	**97.9 ± 7.7**
TZ17	px	854	2.85 ± 0.20	56.7 ± 5.1	14.31 ± 0.82	6.30[a]	8.10	-	32.9 ± 5.7
	px	114	3.3593 ± 0.0020	58.9 ± 2.9	12.65 ± 0.62	6.30[a]	8.10	-	30.7 ± 3.5
	px	149	3.1723 ± 0.0029	59.4 ± 2.7	13.51 ± 0.61	6.30[a]	8.10	-	32.9 ± 3.3
									32.1 ± 2.2
	ol	172	0.3667 ± 0.0025	38.1 ± 1.4	75.0 ± 2.7	6.30[a]	3.78	-	35.4 ± 1.4
	ol	165	0.2970 ± 0.0020	42.4 ± 1.1	103.1 ± 2.9	6.30[a]	3.78	-	40.4 ± 1.2
	ol	73	0.3534 ± 0.0048	40.4 ± 1.9	82.5 ± 4.0	6.30[a]	3.78	-	37.9 ± 1.9
	ol	358	0.31599 ± 0.00028	32.3 ± 0.9	73.8 ± 2.1	6.30[a]	3.78	-	30.1 ± 0.9
	ol	278	0.24092 ± 0.00049	32.9 ± 1.0	98.5 ± 3.1	6.30[a]	3.78	-	31.3 ± 1.0
									34.88 ± 0.54
TZ15	px	304	0.63351 ± 0.00098	18.8 ± 1.1	22.7 ± 1.3	6.40[b]	6.35	-	16.1 ± 1.3
	px	234	0.5492 ± 0.0012	17.7 ± 1.5	24.8 ± 2.1	6.40[b]	6.35	-	15.8 ± 1.6
	px*	1500	0.564 ± 0.020	17.6 ± 1.1	22.5 ± 1.6	6.40[b]	6.35	-	15.6 ± 1.2
									15.84 ± 0.78
	ol	292	0.36712 ± 0.00038	13.8 ± 0.5	27.0 ± 1.1	6.40[b]	4.76	-	12.73 ± 0.65
	ol	301	0.42359 ± 0.00090	16.0 ± 1.3	29.0 ± 2.3	6.40[b]	4.76	-	14.4 ± 1.4
									13.13 ± 0.59
TZ19	px	332	1.7166 ± 0.0025	37.3 ± 1.1	15.67 ± 0.45	6.13[a]	9.78	-	24.0 ± 1.5
	px	363	1.80594 ± 0.00096	36.9 ± 1.2	14.76 ± 0.47	6.13[a]	9.78	-	22.9 ± 1.6
									23.5 ± 1.1
	ol	392	0.24767 ± 0.00067	24.68 ± 0.59	71.9 ± 1.7	6.13[a]	3.07	-	22.99 ± 0.59
	ol	272	0.23623 ± 0.00037	23.9 ± 1.1	73.1 ± 3.2	6.13[a]	3.07	-	22.3 ± 1.1
									22.84 ± 0.52

[a] Calculated from isochron intercepts (procedure of Blard and Pik, 2008) (Fig. A2).

[b] Equal to the mean $(^3He/^4He)_{mag}$ value of all other samples (6.40 R_A).

Table A4: Neon data for pyroxene and olivine separates. Extractions were performed by step-wise heating at GFZ Potsdam and measured using a VG-5400 noble gas mass spectrometer. Data have been corrected for isobaric interferences, mass-discrimination effects and analytical blanks (see text). Uncertainties correspond to 1σ.

Sample	sample weight [g]	Temp [°C]	measured ^{20}Ne [10^6 atoms g^{-1}]	measured $^{22}Ne/^{20}Ne$ [10^{-2}]	measured $^{21}Ne/^{20}Ne$ [10^{-3}]	calculated $^{21}Ne_{cos}$ [10^6 atoms g^{-1}]
TZ10 px		900	662 ± 24	10.697 ± 0.070	3.23 ± 0.16	
		1750	1253 ± 38	11.37 ± 0.16	13.61 ± 0.16	
	0.40058	Total	1916 ± 45	11.14 ± 0.11	10.02 ± 0.16	13.52 ± 0.44
TZ12 px		900	1130 ± 33	10.223 ± 0.087	3.05 ± 0.15	
		1750	8270 ± 210	10.437 ± 0.033	4.507 ± 0.060	
	0.5968	Total	9400 ± 210	10.411 ± 0.031	4.332 ± 0.056	12.91 ± 0.60
TZ13 px		900	960 ± 33	10.53 ± 0.17	3.25 ± 0.26	
		1750	1529 ± 49	11.31 ± 0.12	13.66 ± 0.25	
	0.32478	Total	2489 ± 59	11.01 ± 0.10	9.64 ± 0.22	16.62 ± 0.67
TZ14 px		900	1946 ± 53	10.173 ± 0.047	3.05 ± 0.11	
		1750	1659 ± 48	11.35 ± 0.066	14.28 ± 0.22	
	0.50456	Total	3605 ± 72	10.715 ± 0.041	8.22 ± 0.16	18.96 ± 0.69
TZ17 px		900	4710 ± 120	10.074 ± 0.028	2.960 ± 0.058	
		1750	6870 ± 180	10.160 ± 0.028	3.876 ± 0.064	
	0.8542	Total	11580 ± 220	10.125 ± 0.020	3.503 ± 0.045	6.30 ± 0.53
TZ15 px		900	931 ± 25	10.088 ± 0.052	3.023 ± 0.080	
		1750	766 ± 20	10.380 ± 0.065	6.53 ± 0.12	
	1.50078	Total	1697 ± 32	10.220 ± 0.041	4.606 ± 0.077	2.79 ± 0.14
TZ10 ol		900	95 ± 14	12.63 ± 0.54	22.3 ± 3.3	
		1750	650 ± 26	14.44 ± 0.18	41.3 ± 1.2	
	0.4192	Total	745 ± 30	14.21 ± 0.17	38.9 ± 1.2	26.8 ± 1.4
TZ12 ol		900	166.5 ± 5.0	11.37 ± 0.25	13.83 ± 0.82	
		1750	443 ± 19	15.68 ± 0.24	54.8 ± 2.0	
	0.40132	Total	609 ± 20	14.50 ± 0.19	43.6 ± 1.5	24.8 ± 1.2
TZ13 ol		900	69 ± 13	15.9 ± 1.1	47.7 ± 8.1	
		1750	783 ± 26	14.68 ± 0.24	40.98 ± 0.86	
	0.45104	Total	852 ± 29	14.78 ± 0.24	41.5 ± 1.0	32.8 ± 1.4
TZ14 ol		900	155.1 ± 5.7	11.07 ± 0.21	10.55 ± 0.51	
		1750	519 ± 28	16.71 ± 0.46	67.8 ± 3.0	
	0.24534	Total	674 ± 29	15.41 ± 0.36	54.6 ± 2.4	34.9 ± 2.2

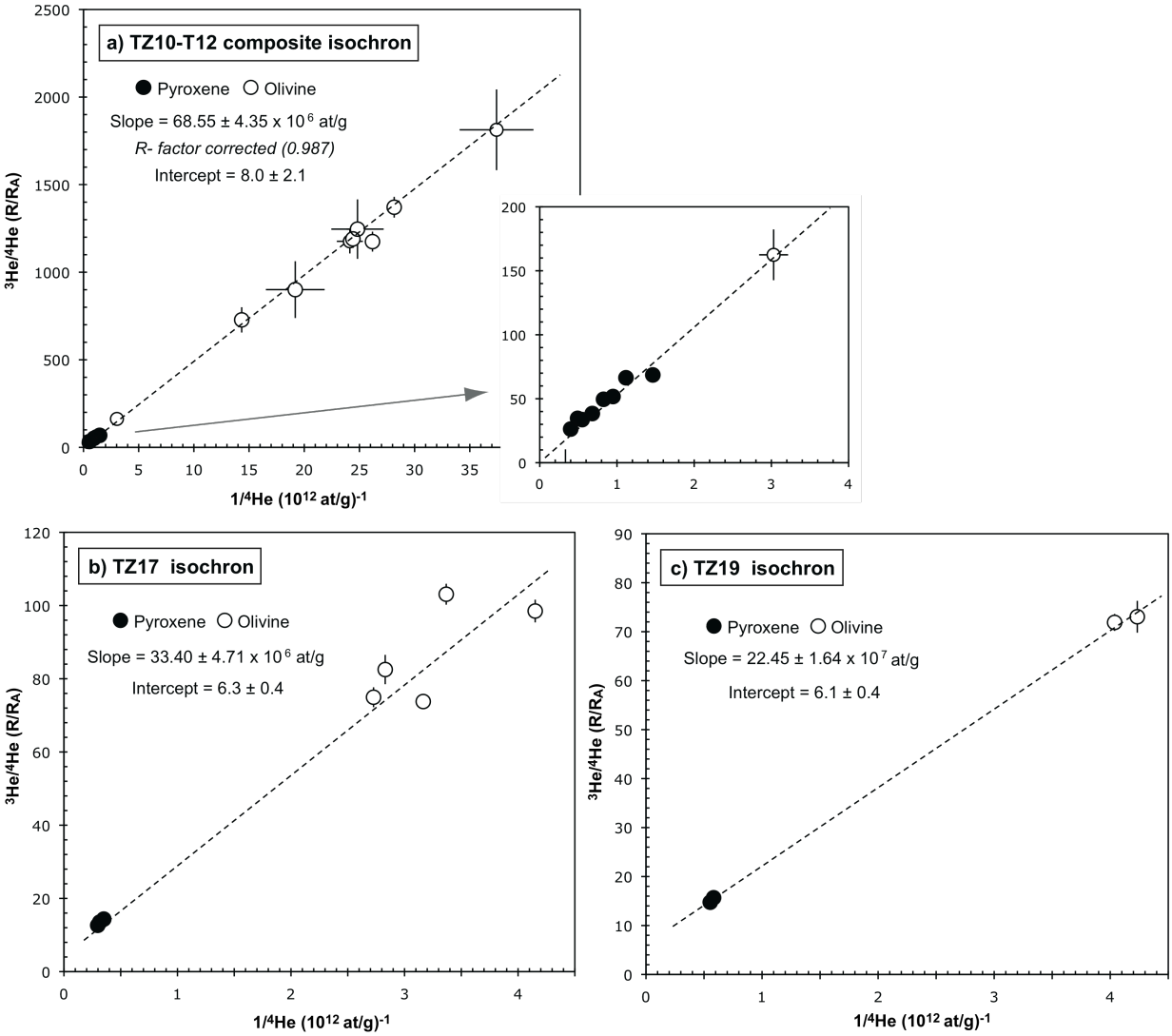

Fig. A2: ^{3}He-^{4}He isochron plots for samples (a) TZ10 and TZ12, (b) TZ17 and (c) TZ19. The slope in each plot corresponds to the cosmogenic ^{3}He concentration in the sample, while the intercept represents its magmatic ^{3}He/^{4}He ratio. The magmatic ^{3}He/^{4}He ratios of samples TZ17 and TZ19 were determined by this method. For all samples, final calculations of cosmogenic ^{3}He were made using the traditional procedure (see section 3.3 in main text). The isochrons for samples TZ10 and TZ12, which were taken from the same lava flow, allow comparison of the results with those of the traditional procedure (Table A3).

Table A5: $^{40}Ar/^{39}Ar$ data for sample TZ15.

Incremental Heating			36Ar(a)	37Ar(ca)	38Ar(cl)	39Ar(k)	40Ar(r)	Age ± 1σ (Ka)	40Ar(r) (%)	39Ar(k) (%)	K/Ca ± 1σ
06MQ114	650 °C		0.002716	0.000407	0.000027	0.004101	0.009864	1340.4 ± 1856.1	1.21	0.11	4.333 ± 16.140
06MQ115	750 °C		0.003416	0.090309	0.000000	0.177951	0.203728	638.1 ± 39.8	16.79	4.65	0.847 ± 0.050
06MQ116	800 °C	✓	0.001495	0.190794	0.000000	0.523822	0.479927	510.7 ± 12.4	52.02	13.69	1.181 ± 0.061
06MQ117	850 °C	✓	0.002088	0.308397	0.000000	0.927802	0.876304	526.4 ± 8.8	58.61	24.25	1.294 ± 0.068
06MQ118	875 °C	✓	0.000907	0.226277	0.000000	0.777474	0.730698	523.8 ± 8.0	73.06	20.32	1.477 ± 0.080
06MQ119	900 °C	✓	0.000526	0.120779	0.000000	0.499021	0.488720	545.9 ± 13.1	75.76	13.04	1.777 ± 0.098
06MQ120	950 °C	✓	0.000655	0.116930	0.000000	0.457026	0.443540	540.9 ± 13.6	69.53	11.95	1.681 ± 0.090
06MQ121	1025 °C	✓	0.000822	0.102404	0.000000	0.230141	0.220868	534.9 ± 27.2	47.59	6.02	0.966 ± 0.055
06MQ122	1125 °C	✓	0.001268	0.161964	0.000000	0.139859	0.120800	481.4 ± 45.7	24.37	3.66	0.371 ± 0.020
06MQ123	1250 °C		0.002076	1.848403	0.000000	0.088682	0.085227	535.7 ± 89.3	12.20	2.32	0.021 ± 0.001
		Σ	0.015969	3.166665	0.000027	3.825881	3.659677				

Information on Analysis
CR16 basalt gmas furnace BSHS
Project = Tanzania Irradiation = VU57 J = 0.0003090 ± 0.0000009 DRA 1 = 25.260 ± 0.076 Ma

Results	40(r)/39(k) ± 1σ	Age ± 1σ (Ka)	MSWD	39Ar(k) (%,n)	K/Ca ± 1σ
Error Plateau	0.9460 ± 0.0082 ± 0.87%	527.3 ± 4.9 ± 0.92%	1.01	92.92 7	0.670 ± 0.186
		External Error ± 5.0	1.01	Statistical T Ratio	
		Analytical Error ± 4.6	1.0067	Error Magnification	
Total Fusion Age	0.9566 ± 0.0103 ± 1.07%	533.2 ± 5.9 ± 1.12%		10	0.027 ± 0.001
		External Error ± 6.0			
		Analytical Error ± 5.7			

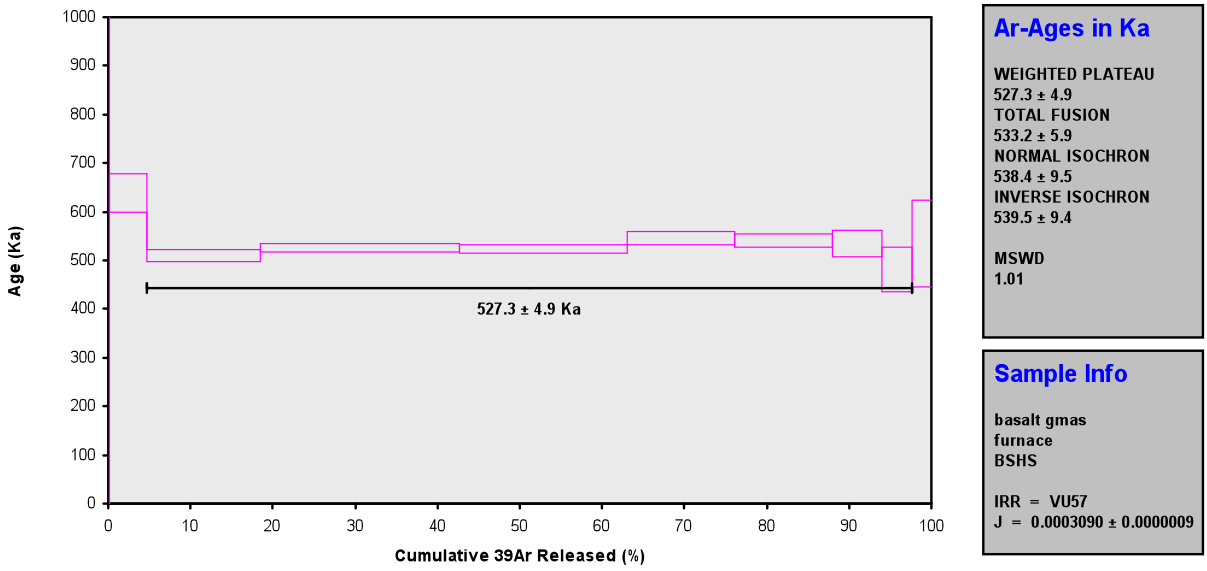

Fig. A3: $^{40}Ar/^{39}Ar$ step heating spectrum for sample TZ15.

References:

Blard, P. H., Pik, R., Lavé, J., Bourlès, D. L., Burnard, P., Yokochi, R., Marty, B., Trusdell, F., 2006. Cosmogenic ^{3}He production rates revisited from evidences of grain size dependent release of matrix-sited helium. Earth and Planetary Science Letters 247 (3-4), 222–234.

Blard, P. H., Pik, R., 2008. An alternative isochron method for measuring cosmogenic ^{3}He in lava flows. Chemical Geology, 251, 20-32.

Farley, K. A., Libarkin, J., Mukhopadhyay, S., Amidon, W., 2006. Cosmogenic and nucleogenic ^{3}He in apatite, titanite, and zircon. Earth and Planetary Science Letters 248 (1-2), 451-461.

Koppers, A.A.P., Staudigel, H., Wijbrans, J.R. 2000. Dating crystalline groundmass separates of altered Cretaceous seamount basalts by the Ar-40/Ar-39 incremental heating technique. Chemical Geology 166, 139–158.

Matsuda, J., Matsumoto, T., Sumino, H., Nagao, K., Yamamoto, J., Miura, Y., Kaneoka, I., Takahata, N., Sano, Y., 2002. The ^{3}He/^{4}He ratio of the new internal He Standard of Japan (HESJ). Geochemical Journal 36, 191–195.

Niedermann, S., Graf, T., Marti, K., 1993. Mass spectrometric identification of cosmic-ray-produced neon in terrestrial rocks with multiple neon components. Earth and Planetary Science Letters 118, 65-73.

Niedermann, S., Bach, W., Erzinger, J., 1997. Noble gas evidence for a lower mantle component in MORBs from the southern East Pacific Rise: Decoupling of helium and neon isotope systematics. Geochimica et Cosmochimica Acta 61 (13), 2697-2715.

Pik, R., Marty, B., Hilton, D., 2006. How many mantle plumes in Africa? The geochemical point of view. Chemical Geology 226 (3-4), 100-114, special Issue in Honour of R.K. O'Nions.

Schneider, B., Kuiper, K., Postma, O., Wijbrans, J., 2009. ^{40}Ar/^{39}Ar geochronology using a quadrupole mass spectrometer. Quaternary Geochronology 4 (6), 508–516.

Zimmermann, L., Blard, P.H., Burnard, B., Medynski, S., Pik, R., Puchol, N. A new ultra-high vacuum, single vacuum furnace design for cosmogenic ^{3}He extraction. Submitted to Geostandards and Geoanalytical Research.